(2)

PL-TR-93-2231

A MODEL OF THE ATMOSPHERIC METAL DEPOSITION BY COSMIC DUST PARTICLES

W. J. McNeil

Radex, Inc.
Three Preston Court
Bedford, MA 01730

November 17, 1993

Scientific Report No. 3

Approved for public release; distribution unlimited

PHILLIPS LABORATORY
Directorate of Geophysics
AIR FORCE MATERIEL COMMAND
HANSCOM AIR FORCE BASE, MA 01731-3010

"This technical report has been reviewed and is approved for publication"

EDWARD C. ROBINSON
Contract Manager
Data Analysis Division

ROBERT E. McINERNEY, Director
Data Analysis Division

This report has been reviewed by the ESD Public Affairs Office (PA) and is releasable to the National Technical Information Service (NTIS).

Qualified requestors may obtain additional copies from the Defense Technical Information Center. All others should apply to the National Technical Information Service.

If your address has changed, or if you wish to be removed from the mailing list, or if the addressee is no longer employed by your organization, please notify PL/TSI, 29 Randolph Road, Hanscom AFB, MA 01731-3010. This will assist us in maintaining a current mailing list.

Do not return copies of this report unless contractual obligations or notices on a specific document requires that it be returned.

REPORT DOCUMENTATION PAGE

Form Approved
OMB No. 0704-0188

1. AGENCY USE ONLY *(Leave blank)*

2. REPORT DATE
17 November 1993

3. REPORT TYPE AND DATES COVERED
Scientific Report No. 3

4. TITLE AND SUBTITLE
A Model of the Atmospheric Metal Deposition by Cosmic Dust Particles

5. FUNDING NUMBERS
PE 63220C
PR 7659 TA GY WU AA

Contract F19628-93-C-0023

6. AUTHOR(S)
W. J. McNeil

7. PERFORMING ORGANIZATION NAME(S) AND ADDRESS(ES)
RADEX, Inc.
Three Preston Court
Bedford, MA 01730

8. PERFORMING ORGANIZATION REPORT NUMBER
RXR-93111

9. SPONSORING/MONITORING AGENCY NAME(S) AND ADDRESS(ES)
Phillips Laboratory
29 Randolph Road
Hanscom AFB, MA 01731-3010

Contract Manager: Edward Robinson/GPD

10. SPONSORING/MONITORING AGENCY REPORT NUMBER
PL-TR-93-2231

11. SUPPLEMENTARY NOTES

12a. DISTRIBUTION/AVAILABILITY STATEMENT
Approved for Public Release
Distribution Unlimited

12b. DISTRIBUTION CODE

13. ABSTRACT *(Maximum 200 words)*

We have developed a model of the deposition of meteoric metals in Earth's atmosphere. The model takes as input the total mass influx of material to the Earth and calculates the deposition rate at all altitudes through solution of the drag and subliminal equations in a Monte Carlo-type computation. The diffusion equation is then solved to give steady state concentration of complexes of specific metal species and kinetics are added to calculate the concentration of individual complexes. Concentrating on sodium, we calculate the Na(D) nightglow predicted by the model, and by introduction of seasonal variations in lower troposheric ozone based on experimental results, we are able to duplicate the seasonal variation of mid-latitude nightglow data.

14. SUBJECT TERMS
Atmospheric metal deposition, Sodium nightglow, Thermospheric ozone

15. NUMBER OF PAGES
82

16. PRICE CODE

17. SECURITY CLASSIFICATION OF REPORT	18. SECURITY CLASSIFICATION OF THIS PAGE	19. SECURITY CLASSIFICATION OF ABSTRACT	20. LIMITATION OF ABSTRACT
Unclassified	Unclassified	Unclassified	Unlimited

TABLE OF CONTENTS

LIST OF FIGURES

Page

List of Figures (Cont'd)

List of Figures (Cont'd)

Page

LIST OF TABLES

ACKNOWLEDGMENTS

Ed Murad and Shu Lai, PL/WSSI, were instrumental in all phases of this work from conception to completion. We are indebted to them for their technical guidance and critical evaluation. Total ozone data was provided by NCAR, UCAR, Boulder, CO.

1.0 INTRODUCTION

The influx of extra-terrestrial material is responsible for the deposition of some seventeen thousand tons of matter in Earth's atmosphere each year. Among the important consequences of this process is the formation of layers of free metals at around 100 km altitude, where the atmosphere becomes dense enough for substantial ablation of the particles to begin. The appearance of layers of neutral atomic metals, such as sodium, is a result of the combination of the ablation process and atmospheric chemistry. Ablation produces elemental metal atoms. As the metal atoms diffuse downward, they are increasingly subject to three-body reactions as the atmospheric density increases, forming the various metal oxides. From there, a chain of reactions results eventually in the formation of conglomerates, which fall to Earth.

Although the deposition process and the subsequent kinetics of the metals is intimately related, it is often necessary to separate the modeling effort into phases, the first of which produces a source function for the appearance of metal atoms. With this, one can next address the diffusion problem by considering the transport of all species containing a particular metal. This is valid *if* the important chemistry takes place below the turbopause, where atmospheric turbulence leads to a mass independent scale height for minor species. Under these assumptions, the diffusion equation can be solved for the steady state concentration of the total number of atoms containing the metal. Then, a kinetic model can be developed and solved in the steady state to give the relative amount of each particular molecular metal species. Implicit in this solution is the assumption that the removal of all metal molecules is uniform, which is not completely true for the complexes that are the eventual result of the chemistry. The assumption is quite good in the metal layer itself, however, since there diffusion is rapid, compared to the non-diffusive removal mechanisms.

The creation of a model can be divided into three separate problems: the generation of an altitude dependant source function giving the rate of deposition of metal atoms, the solution of the transport equation for the steady state total number density of metal containing species, and the creation of a kinetic model to give the relative amounts of particular species at a particular altitude. Different modelers have in the past approached each of these steps in rather unique ways. For instance, *Plane* [1991], in his model of sodium deposition, considers eddy-diffusion only. This allows the entire diffusion problem to be based on only an assumed flux of sodium containing species at the minimum modeled altitude of 65 km. This flux is chosen so that the model results in a reasonable total column density of free sodium, matching observations. *Thomas, et al.* [1983] began with a source profile calculated by *Hunten, et al.* [1980] which is scaled uniformly with altitude in order to achieve a reasonable free sodium peak height. Both the treatments neglect molecular diffusion, which limits the model to relatively low altitudes.

In the present work, we have attempted to create a self-consistent model, beginning with the equations describing the behavior of meteoric particles in the atmosphere. By following the time behavior of individual particles, we are able to derive the relative amount of material deposited by them at various altitudes. This is then coupled with the estimated size distribution functions of *Hughes* [1992]. A Monte Carlo-type calculation is then performed to give an average deposition as a function of altitude. This is scaled by assuming a total influx of material, estimated by several workers to be around 507 grams per second to give a source function. The source function, obtained in total grams per altitude unit per second, is then applied to a chosen metal species with known average weight percents of the chosen metal.

The source function is then combined with a diffusion model, including both molecular and eddy diffusion, to give steady state concentrations of compounds of the chosen metal. A kinetic model is then added to give absolute concentrations of various metal compounds. We test this model on sodium with particular attention to the variation in sodium night-glow with ozone density. The chemistry of the model is introduced in both a simplistic and a more complicated sequence of reactions, both giving results in good agreement with observations.

2.0 THE DEPOSITION FUNCTION

The first step in the modeling is the calculation of the rate of deposition of metal atoms at a given altitude. The rate of deposition depends on the atmospheric density and the velocity and size of the particle. To a lesser extent, this rate depends on the specific composition of the particle as well, but we neglect this complication for simplicity. The particle is assumed to be spherical in shape and is assumed to be composed of a material like Chondrodite, $[(MgOH)_2 \cdot 2Mg_2SiO_4]$, with a specific gravity ρ_m of 3.2 g/cc. The velocity of the particle is subject to some speculation. If the particle were sitting still relative to the Earth when encountered, the Earth-fixed velocity would be almost 30 km/s. But, according to *Hughes* [1992], most particles are in prograde orbits around the sun (*i.e.*, they revolve around the sun in the same sense as does the Earth). This makes the relative velocity substantially less. Typical geocentric velocities are from 13.8 to 16.2 km/s, again according to *Hughes* [1992]. We will investigate the velocity dependence of deposition and, eventually, find that the completed model is rather insensitive to the precise velocity of the particle.

The evolution of a particle after it enters Earth's atmosphere can be modeled as follows. In a time *dt*, the particle encounters a mass of atmosphere equal to

$$M_a = A(m/\rho_m)^{2/3} \rho_a V dt \tag{1}$$

where ρ_a is the atmospheric density, V is the geocentric velocity, m is the mass of the particle and A is a dimensionless shape factor, equal to about 1.2, which allows the expression to be written in terms of mass and density rather than radius. The impact of the particle with the air serves both to heat the air and the particle, leading to the ablation of metal atoms, and to slow the meteor down. The change in velocity with time contains both the acceleration of the particle due to gravity and the atmospheric drag.

$$\frac{dV}{dt} = -\frac{\Gamma A \rho_a V^2}{m^{1/3}\rho_m^{2/3}} + \frac{\mu}{(h-h_0)^2} \tag{2}$$

where the first term is the usual expression for drag, an empirical relationship, and the second term is the acceleration of gravity. *Hughes* [1992] gives a range from 0.5 to 1.0 for Γ and we choose to fix the value at 0.75 in this model. The acceleration due to gravity, μ, is 4.0(20) cm^3/s^2.

The maximum possible energy released in the air/particle collision is equal to the energy that would be imparted to the air molecules if they were raised to a velocity equal to the particle velocity, or,

$$E_{\max} = \frac{1}{2} A (m/\rho_m)^{2/3} V^3 \tag{3}$$

which follows from Eq(1). It is assumed that some fraction of this energy, Λ, goes toward heating the material in the particle instead of toward heating the air. With this, one can write the mass loss due to ablation as

$$\frac{dm}{dt} = -\frac{\Lambda A m^{2/3} \rho_a V^3}{2\xi \rho_m^{2/3}} \tag{4}$$

where ξ is the heat of sublimation, equal to around 5(10) erg/g. *Hughes* [1992] gives a range for Λ from 0.1 to 0.6. We fix Λ at 0.2.

With Eq(2) and Eq(4), along with the time dependent equation for altitude,

$$\frac{dh}{dt} = V \tag{5}$$

we are able to solve for the velocity, altitude, and mass of a particle at any time, given its initial velocity and mass. The only element missing is the atmospheric density ρ_a. We have modeled this after data presented by *Kelly* [1989] for sunspot maximum. Figure 1 shows the model density in g/cc.

We used a standard 4-th order Runge-Kutta integrator to solve Eq(2), Eq(4), and Eq(5) simultaneously. Figure 2 shows a typical plot for an initial mass of one gram, with the initial velocity varied between 10 and 20 km/s. Above about 90 km, there is little ablation due to the

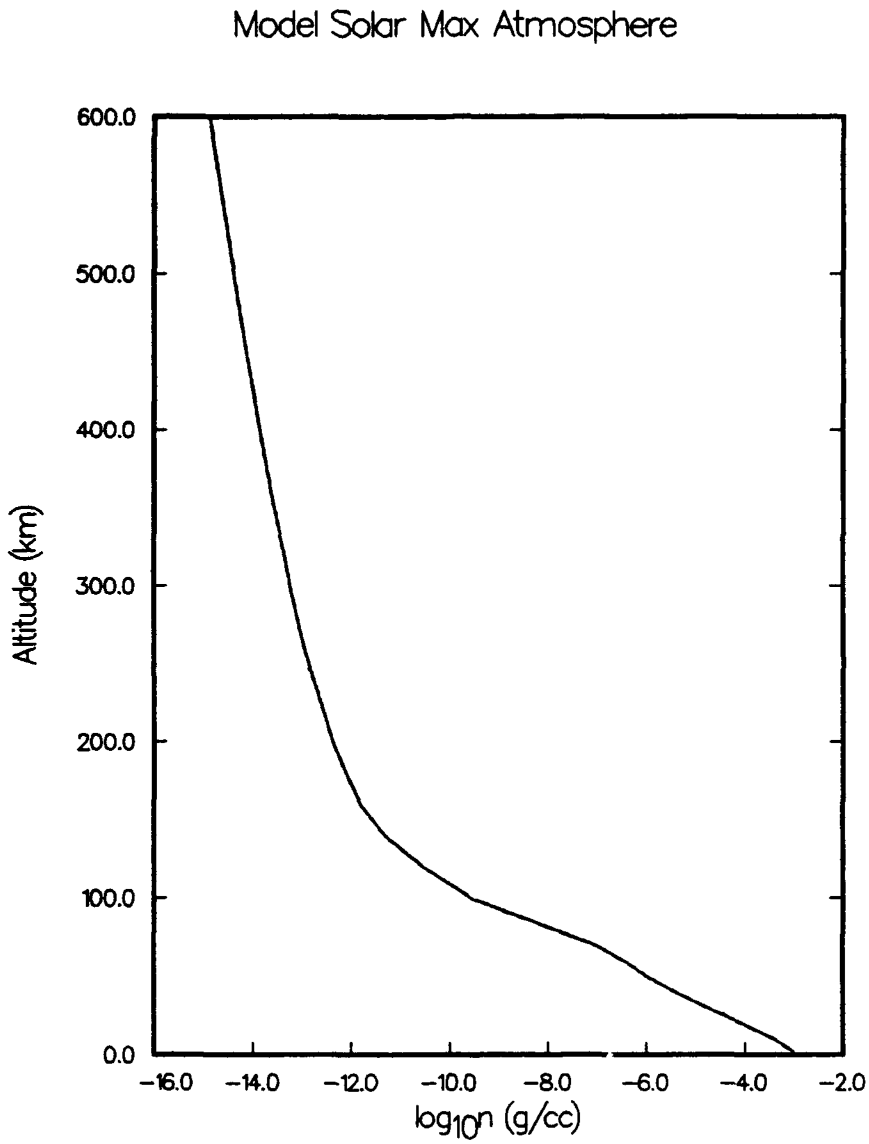

Figure 1. The modeled density of the atmosphere for solar maximum conditions [*after Kelly*, 1989].

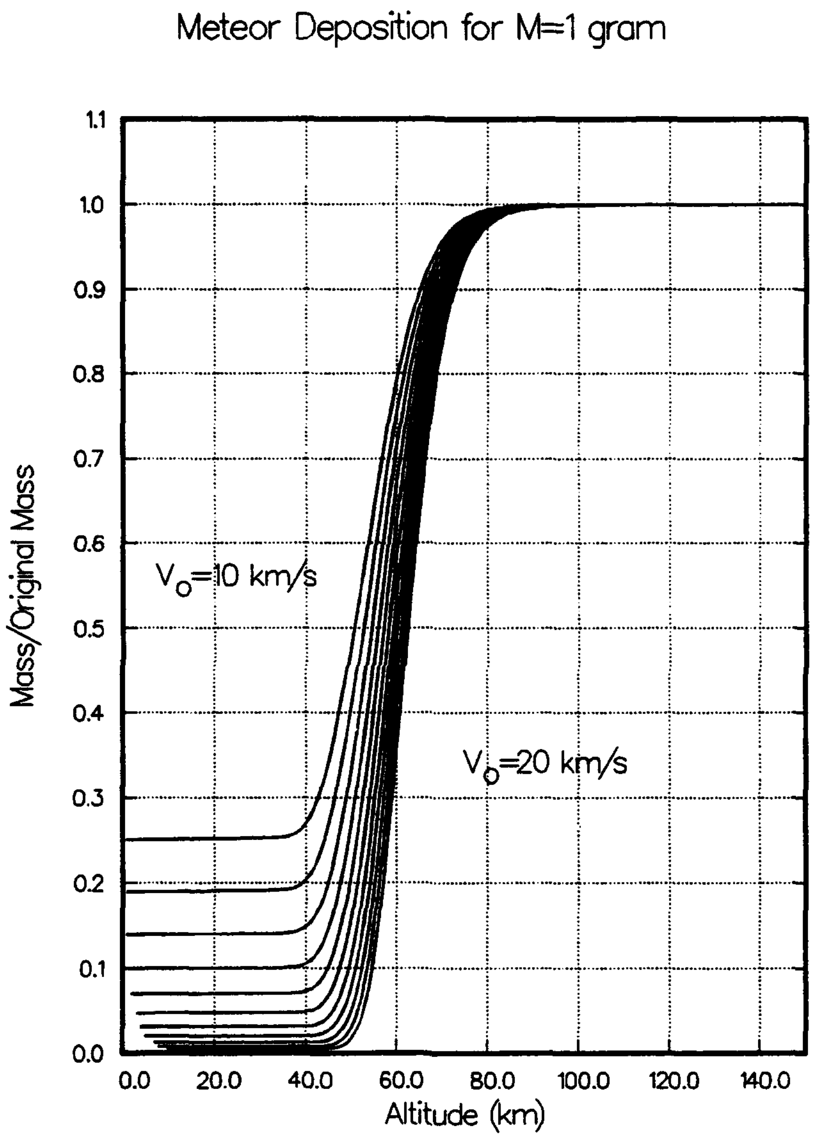

Figure 2. **Meteor mass, normalized to initial mass, at various altitudes for an initial mass of one gram.**

low atmospheric density. The bulk of the ablation takes place between 50 and 80 km altitude. Also, below about 50 km altitude, there appears to be a terminal velocity. The mass is not, in fact, precisely constant. However, the vary rapid deceleration which takes place as the atmosphere begins to become substantial effectively shuts off ablation below about 50 km. This also greatly reduces the particle velocity, which would explain why meteoric particles of mass less than a few grams are only luke-warm when they reach Earth.

The altitude at which the majority of mass loss takes place depends greatly on the initial mass, however, the ratio of terminal mass to initial mass does not vary greatly with terminal mass. Figure 3 shows the mass profiles for a particle originally 1(-5) grams in mass. The greatest difference between this and the 1 gram meteor is that the lighter meteor ablates at higher altitudes. The ablation for the 1(-5) gram particle takes place between about 70 and 110 km altitude. The mass range from about 1(-8) to 1 gram is the most important region for this modeling, since this range contains the bulk of the influx material. However, it is interesting to observe this behavior in extremes. The largest meteorite fall in the British Isles was the 48 kg meteorite in Limerick in 1813 [*Hughes*, 1991]. Assuming an initial velocity of 10 km/s, this meteor would have ceased to ablate at around 10 km altitude and would have slowed to about 70 m/s at impact. An extremely large meteor, on the other hand, would not decelerate appreciably before reaching Earth's surface. This can be thought of as an extension of the behavior shown in Figures 2 and 3, in which the region of ablation falls below zero altitude.

The variation of ablation with initial velocity is also evident from Figures 2 and 3. There are two main effects. First, the fastest particles lose nearly all their mass by the time they reach the ground. The slowest, however, lose only about 75% of their original mass. Also, faster particles ablate at slightly higher altitudes. The distribution of particle velocities is actually a very poorly known quantity. We would therefore prefer a model which is not too strongly dependent on the initial velocity. We will be able to factor out the first of these effects in the model. The precise altitude of ablation, however, will always be dependent on the choice for the initial velocity. As we go along, we will often present results for initial velocities of 12, 14 and 16 km/s, presuming that these represent minimum, average and maximum values. If we assume, then, that the calculation can be carried out with a single initial velocity, the total deposition can be modeled from the distribution of initial mass. Fortunately, this distribution is a better known quantity than is the initial velocity distribution.

The calculation of the total deposition at a specific altitude is quite straightforward, if we know the distribution of particle mass (frequently called Θ). *Hughes* [1975] has presented a detailed study of the size distribution function and has suggested parameterizations of $\log_{10}\Theta$ that are linear in $\log_{10}m$. We have carried out fits to his data, giving the following functions over three mass ranges.

$$\log_{10}\Theta = -10.08 - 0.550 \log_{10}m \qquad 10(-14) < m < 10(-06)$$
$$\log_{10}\Theta = -14.61 - 1.305 \log_{10}m \qquad 10(-06) < m < 10(-02)$$
$$\log_{10}\Theta = -15.00 - 1.500 \log_{10}m \qquad 10(-02) < m < 10(2)$$

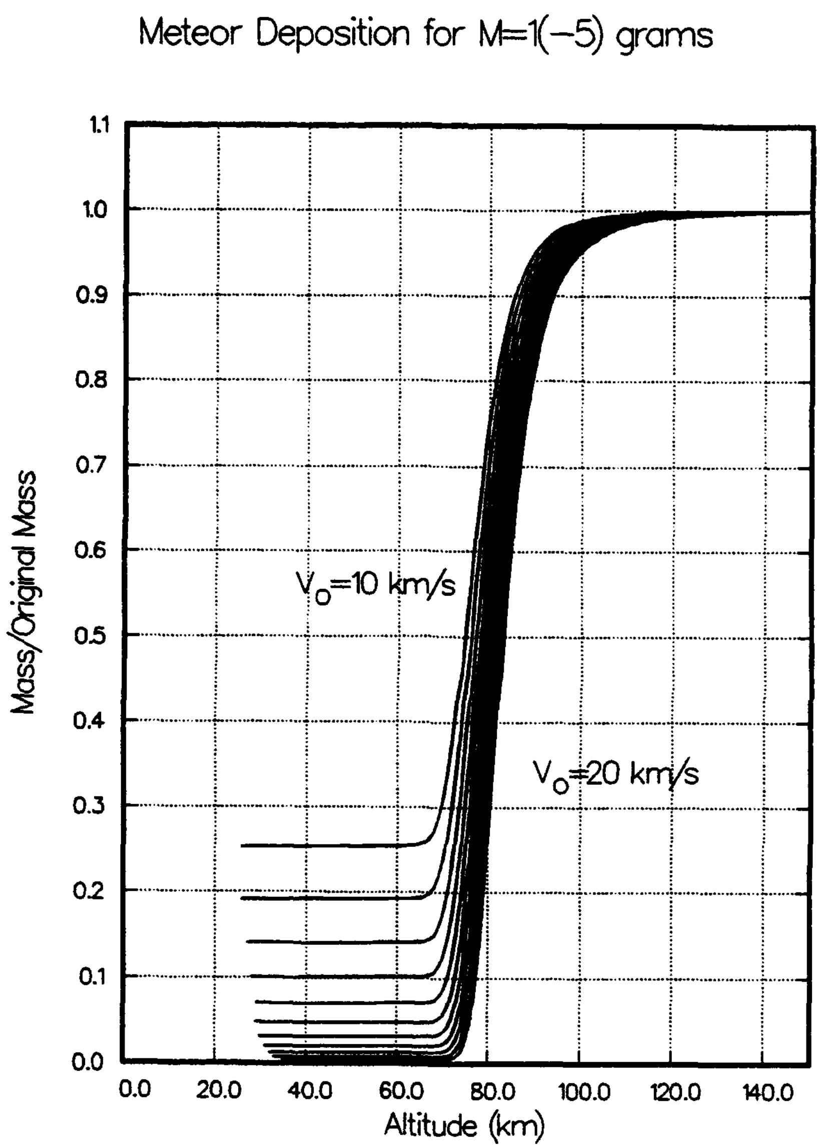

Figure 3. Same as Figure 2, but with an initial mass of 10^{-5} grams.

$\Theta(m)$ is in the form of cumulative number flux of particles greater than the mass m.

Figure 4 shows the cumulative flux model, the units of which are particles-m^{-2}-s^{-1}-2π-str^{-1}. The actual units will not be of use to us, since we will normalize to the total influx after the calculation of relative deposition. Figure 5 shows the relative number of particles at a chosen mass, multiplied by the mass. This essentially gives the contribution of a particle of mass m to the total influx of mass. Figure 5 shows that particles between about 10(-7) and 10(-2) grams make up the major contributors to the mass influx to the Earth.

Now, to perform the calculation of deposition, we will divide altitude into a series of bins, each of which are 1 km in height. Beginning at some high altitude, we will select representative particles from 10(-14) grams to 10(2) grams uniformly represented in $\log_{10}$ m. We will follow each of these representative particles as they descend through the atmosphere. At each time step, we will determine which altitude bin the particle is in, and will accumulate within that bin the mass lost in the present timestep. This is equal to

$$\Delta m = \frac{dm}{dt} \Delta t \, W(m) \qquad (6)$$

where dm/dt is given by Eq(4) and W(m) is a weight function proportional to the relative number of particles of a particular mass. Numerically,

$$W(m) = \Theta(m) - \Theta(m+\delta m) \qquad (7)$$

δm is a computational parameter representing the mass step in $\log_{10}$ space. We choose δm to be 0.1 for the most detailed calculations. Along with the altitude bins, we also accumulate the total mass released by the particle. To this, we add the mass remaining when the particle hits the ground to find the total mass deposited by this particle. This is multiplied by the weight function and summed for all representative particles in the ensemble.

Now, according to several authors [*Hughes*, 1975] the total influx to the Earth of interplanetary matter is around 507 grams/sec, give or take perhaps 150 grams/sec. Therefore, we can normalize the total influx calculated in the model to this value and, if we normalize the altitude dependent accumulations by the same factor, the result will be the deposition rate in each individual altitude bin. The validity of this approach is perhaps best shown by the following reasoning. The accumulations in the altitude bins give the amount of matter deposited in a particular bin relative to the total matter entering the atmosphere. This is already weighted for the known distribution of incoming masses. The normalization of the altitude dependent depositions and total mass accumulated in the calculation, which can be thought of as taking place over some unspecified time interval, to the known total mass influx makes the altitude dependent results equal to the deposition rate.

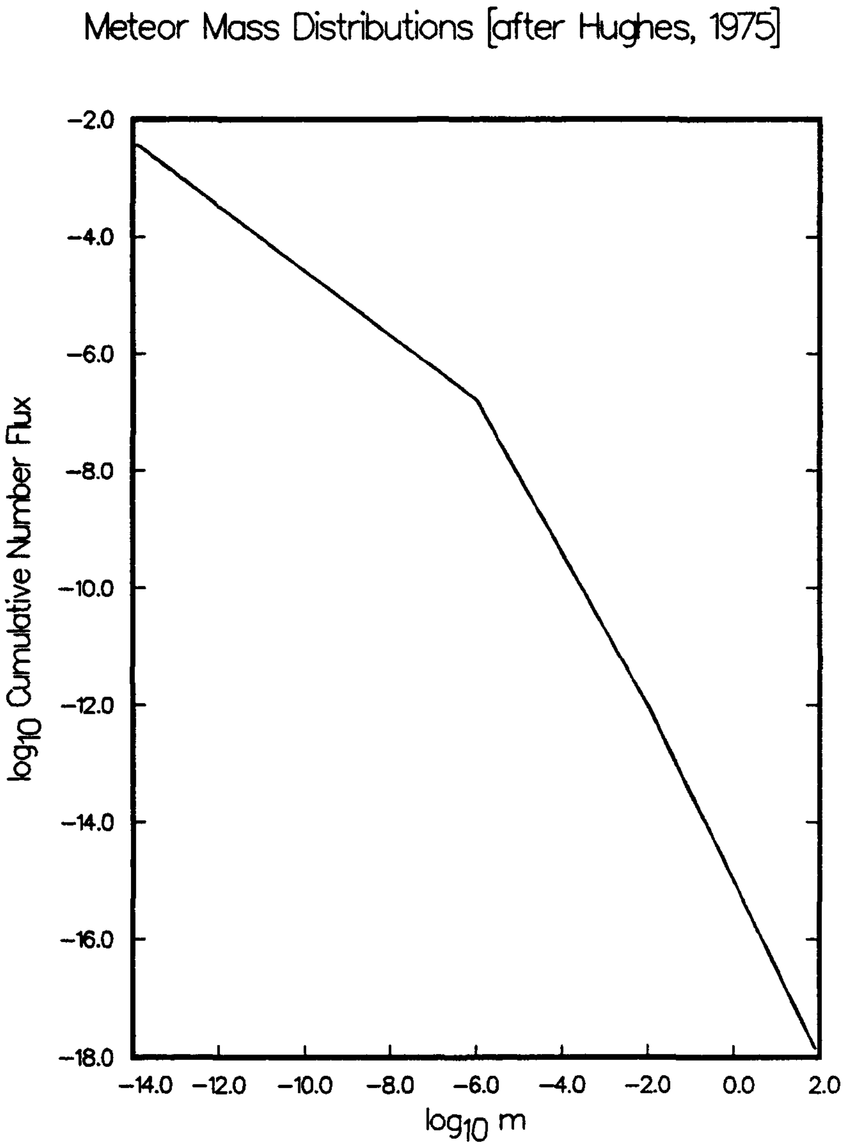

Figure 4. **The distribution of meteor mass, expressed as the number flux of particles greater than or equal to m.**

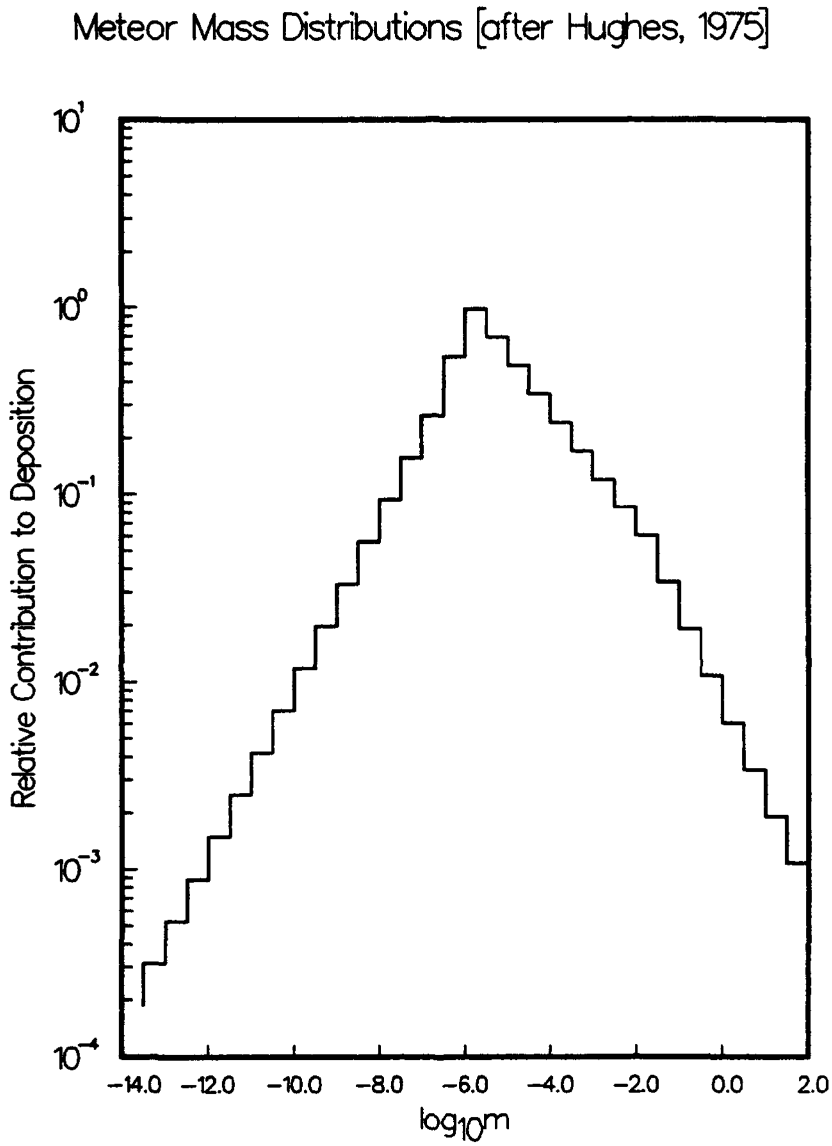

Figure 5. The relative contribution of a meteor of mass m to the total mass influx, calculated from the model in Figure 4.

From there, we divide by the volume of the altitude bin to obtain the grams of meteoric material deposited per cc at individual altitudes. Next, we use meteoric composition data given by *Plane* [1991] to get the deposition rate in atoms/cc. The weight percent and molecular weights of major metallic components of meteoric material are given in Table 1.

TABLE 1. Meteoric Metal Composition

Metal	wt. %	MW
Na	0.6	23.0
Ca	1.0	40.1
Ni	1.5	58.7
Al	1.7	27.0
Fe	11.5	55.8
Mg	12.5	24.3

This concludes the calculation of the deposition rate of metals. The computation itself is rather intensive, requiring about four hours on a Sun workstation. The time required, of course, depends on the choice of the integration time step and the mass time step δm. We have investigated the dependence of the calculations on both these parameters. In the calculation, the integration timestep is chosen such that there will be 200 Runge-Kutta steps for each kilometer of altitude. This depends, of course, on the present velocity of the particle. The mass step δm is chosen to be 0.1. This gives 140 representative particles in the calculation from $\log_{10} m = -14$ to $\log_{10} m = 2$. δm was chosen small enough so that the differences in ablation height were essentially smoothed out over the 1 km altitude bins, leading to a smooth deposition function with altitude. The choice of δm does not significantly affect the deposition rate at a particular altitude, as long as the deposition rate is smooth with altitude, since the deposition at all altitudes is normalized to the known total deposition at the end of the calculation. A final parameter in the calculation is the starting altitude of the particles. We have found that starting them at 600 km is high enough so that there is no significant change in the results that would have been obtained if they were started instead at 500 km.

The deposition function will be called q(h) in what follows, with h the altitude. Figure 6 shows q(h) for sodium with an initial particle velocity of 12 km/s. Recall that we do not attempt to include variations in initial velocity due to the lack of knowledge of the true distribution. Instead, we set the initial velocity and investigate the effects of changes in it on the final results of the model. Figure 7 shows a blow-up of the same q(h). The shape of q(h) is really quite similar to that of the atmospheric density (see Figure 1), at least until the ablation has ceased, at which time q(h) rapidly goes to zero. The peak ablation rate for $V_0 = 14$ km/s is around 75 km altitude with a rate of a little more than 2(-2) atoms/cm^3-s. Figure 8 shows the identical plot for $V_0 = 12$ km/s. The position of the peak is little changed in altitude, but the deposition rate

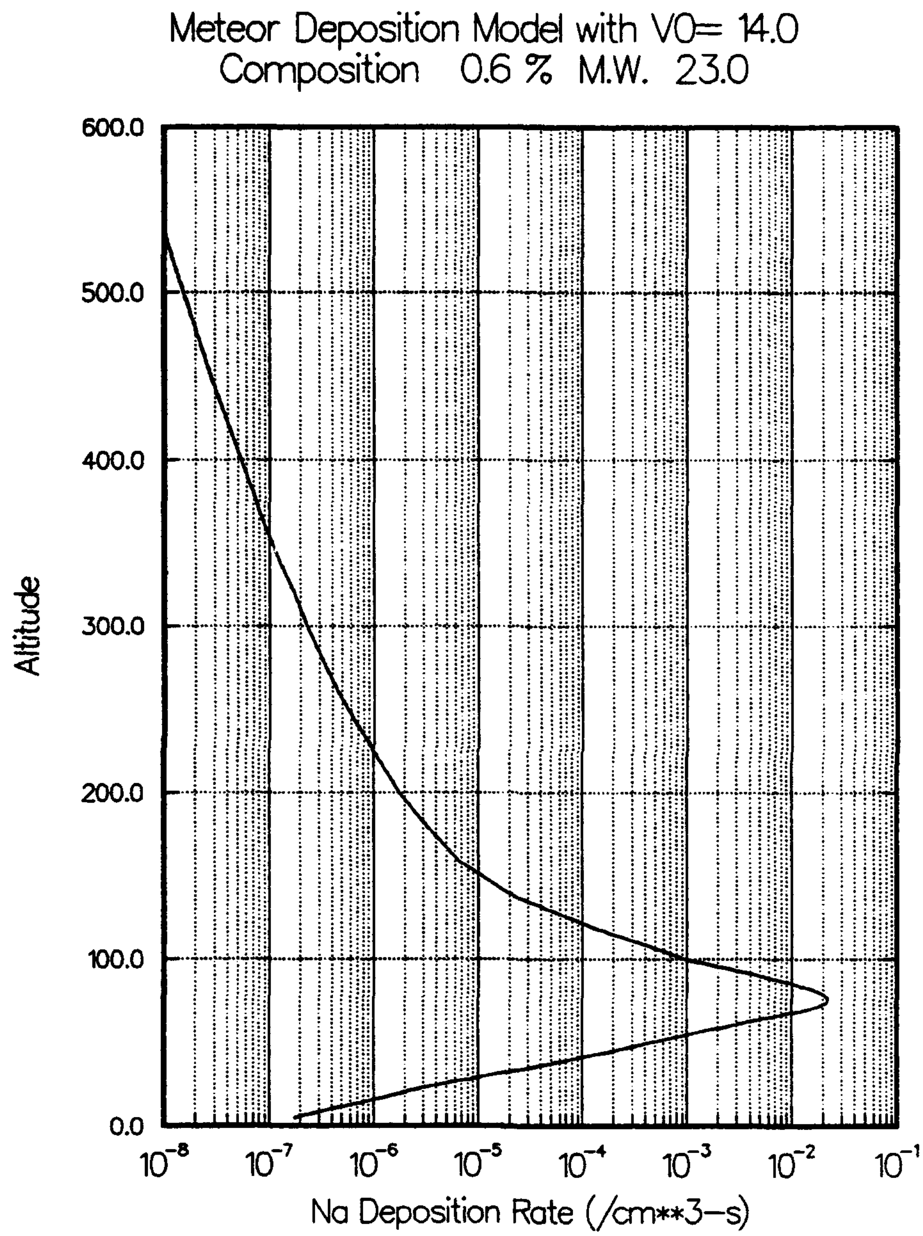

Figure 6. **The calculated deposition rate function for sodium, assuming an initial particle velocity of 14 km/s.**

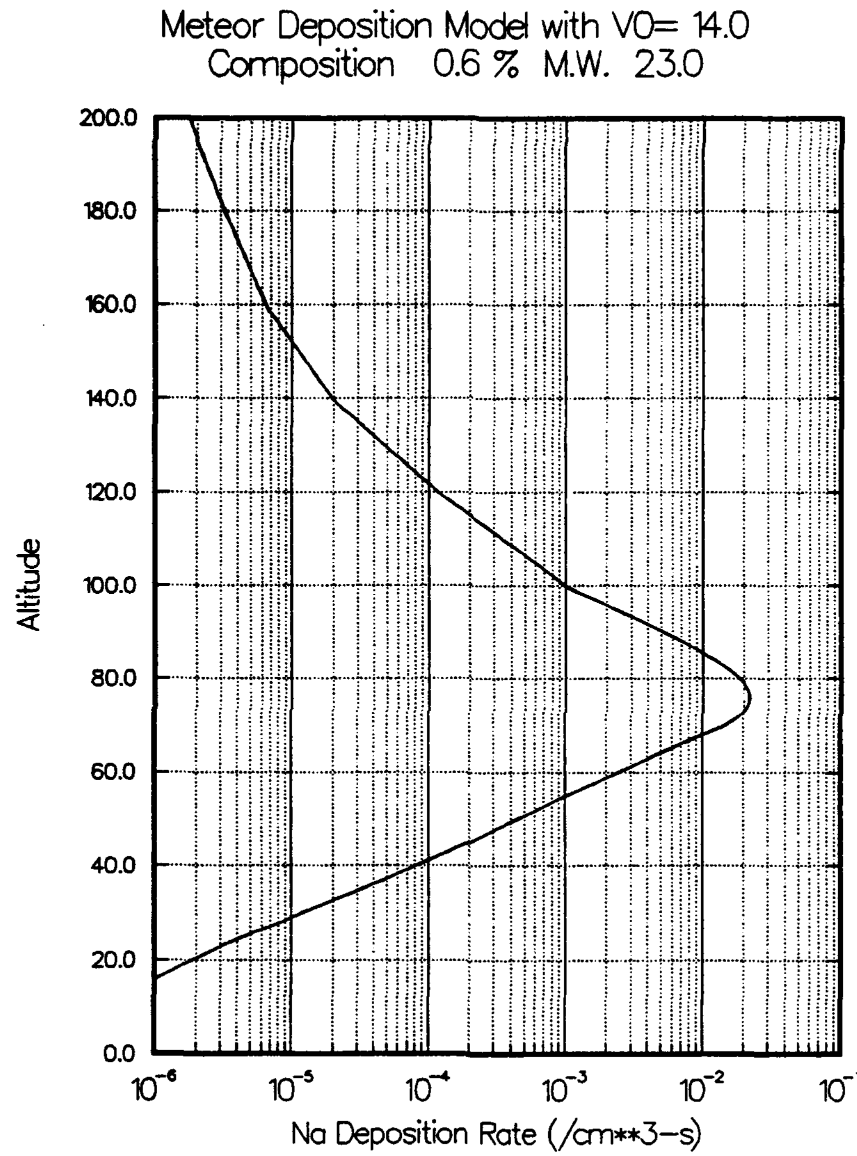

Figure 7. Same as Figure 6, but a blow-up of the region of substantial Na deposition.

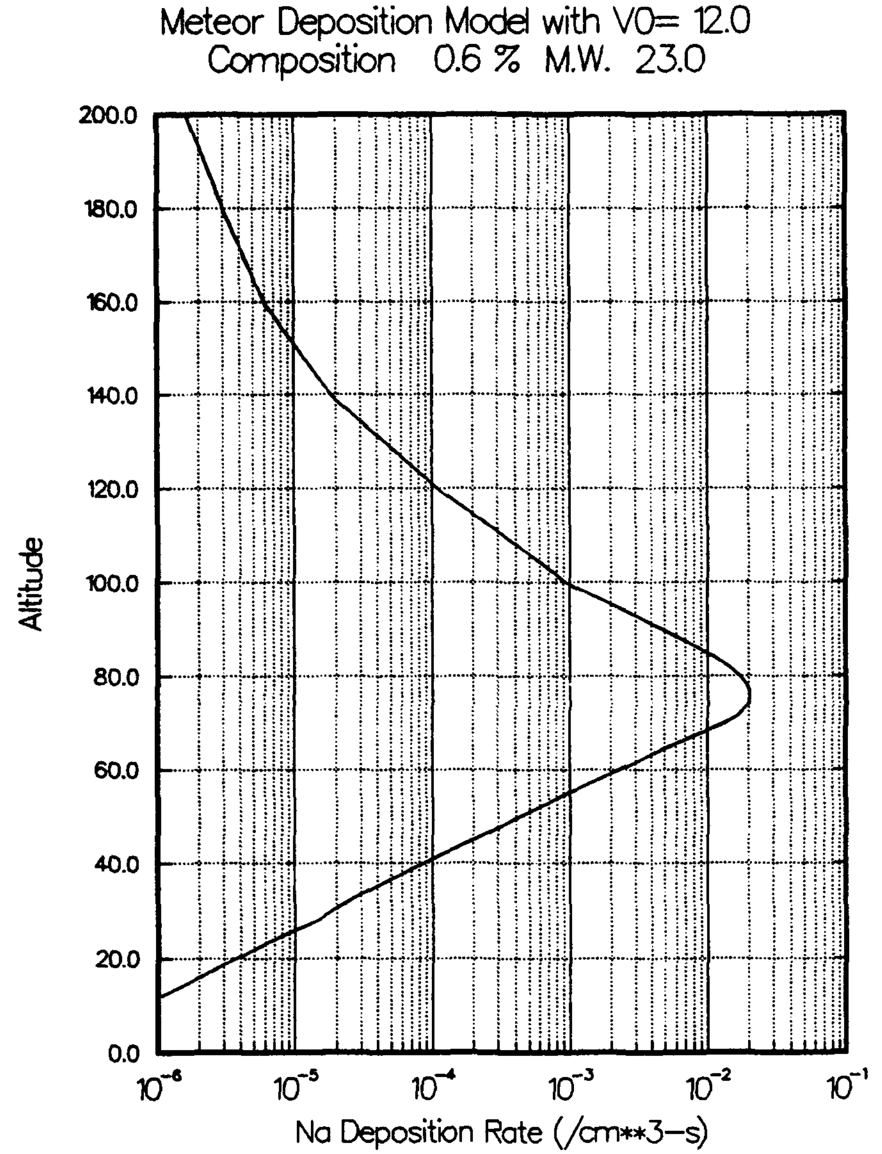

Figure 8. Same as Figure 7, but with an initial particle velocity of 12 km/s.

has fallen slightly, by about 5%. We will not dwell on the comparison of results for various V_0 values at this point, since as we will see, q(h) will go through two further integrations before it becomes a sodium density. It will be more expedient to wait until the final desired quantity is calculated before doing further comparisons. Also, we will not introduce the results for other metals here, since they differ from sodium only by a scale factor which can be calculated easily from the data in Table 1.

Before moving on to the diffusion problem, we will perform one more calculation with q(h). The end product of this model is a steady state density of various sodium species, NaX, where X represents any of the possible sodium species present in the atmosphere. The time dependent diffusion problem

$$\frac{\partial n}{\partial t} + \frac{\partial}{\partial n}(nw) = q(h) \tag{8}$$

where w is the transport velocity and n the concentration of NaX, is quite difficult to solve in general and, even if we did, we would still want to carry out the calculation for a very long time until steady state densities were obtained. Thus, we seek instead a solution to the steady state problem from the outset. In order to remove the time dependence from q(h), we notice that in the steady state, the flux of NaX through one cm^2 at an altitude h must equal the rate of creation at all points above this altitude. If this were not so, the total amount of NaX above any particular altitude could not remain constant. In fact, since Na is injected at all altitudes, it must be that the net flux of NaX is downward at all altitudes. Otherwise, a steady state would not be possible. Therefore, we will concentrate on the quantity F(h), the downward flux of NaX.

It is easy to calculate F(h) from the previous result. By definition, it is equal to the creation rate of Na at all points above the altitude h, *i.e.*,

$$F(h) = \int_h^\infty q(\acute{h})\,d\acute{h} \tag{9}$$

Figure 9 shows F(h) for an initial particle velocity of 14 km/s. As expected, the downward flux is constant below about 60 km, where ablation becomes negligible. Since this calculation requires the substitution of some maximum altitude for infinity in the integral, we show the results of variation in h_{max} in Table 2. Clearly, the maximum of 600 km chosen for the present model is sufficient. For comparison, *Plane* [1991] obtained a value of total sodium flux of 1.3(4) cm^{-2}-s^{-1} from ablation. His result was obtained by adjusting the flux at 65 km solving upward for the total mixing ratio [see *Thomas*, 1974] making the total column density of sodium equal presumed experimental values. We obtain a total downward flux (at ground level) of about 4(4) cm^{-2} s^{-1}, which is about a factor of three larger.

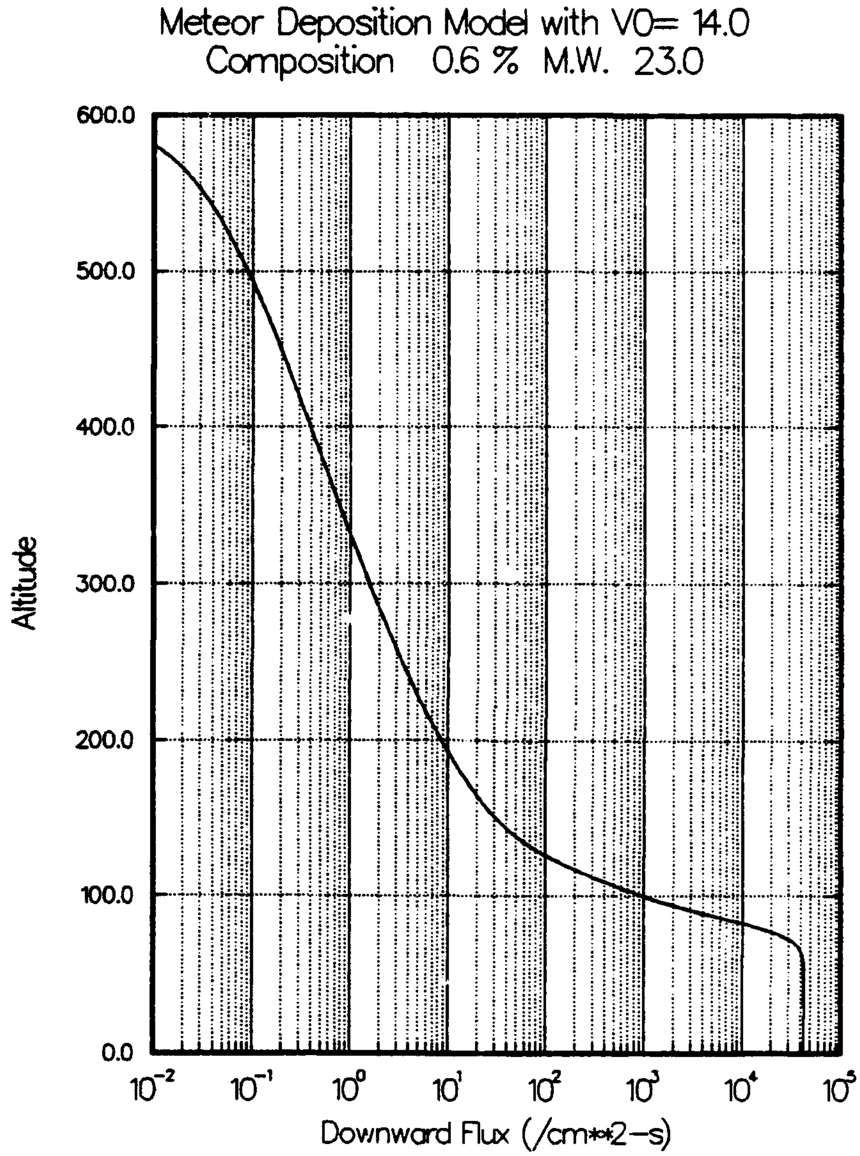

Figure 9. **The downward flux of sodium species NaX, at various altitudes as calculated from the deposition model with V_o = 14 km/s.**

TABLE 2. Variation of Downward Flux ($/cm^2$-s) with Integration Cutoff h_{max}

Downward Flux at	h_{max}=600 km	h_{max}=500 km	h_{max}=400 km
1 km altitude	42769.29	42769.29	42768.98
100 km altitude	943.0632	943.9738	943.6765

Again, as with q(h), we will not investigate the dependence of the solution on the choice for initial particle velocity, leaving the final test of significance until we obtain chemical species densities. We are now ready to move on to the treatment of the solution of the steady state diffusion equation.

3.0 DIFFUSION

The next step in modeling is to derive from the source function a steady state concentration of NaX at various altitudes. By solving for the total concentration of Na species, we avoid at this point the complications of the kinetic reactions. This approach to the problem also allows us to solve for only one minor atmospheric constituent, NaX. At each altitude, the source of NaX is the flux from altitudes above and the sink downward diffusion. In general, the bulk motion of the NaX depends on pressure gradients, concentration gradients, thermal gradients, and differential scale heights. When a species is a minor constituent of the atmosphere, as is NaX, the diffusion problem can be simplified so that the transport velocity w can be written in terms of the concentration gradient of NaX, the scale height of the bulk of the atmosphere, the scale height of NaX, and the temperature gradient. Following *Banks and Kockarts* [1973], the expression is

$$w = -D_{12}\left[\frac{1}{n_1}\frac{dn_1}{dh} + \frac{1}{H_1} + (1+\alpha_T)\frac{1}{T}\frac{dT}{dh}\right] - K\left[\frac{1}{n_1}\frac{dn_1}{dh} + \frac{1}{H} + \frac{1}{T}\frac{dT}{dh}\right] \quad (10)$$

In Eq(10), H_1 is the scale height of NaX, H is the scale height of the atmosphere, D_{12} is the molecular diffusion coefficient, K is the Eddy diffusion coefficient, n_1 is the concentration of NaX, T is the temperature, and h is the altitude.

The mass of NaX enters the equation only in the form of the scale height

$$H_1 = \frac{kT}{m_1 g} \tag{11}$$

with g the acceleration of gravity. The first term in Eq(10) represents molecular diffusion, which predominates at altitudes of above about 100 km. The second term represents Eddy diffusion, predominant in lower altitude regions where turbulence tends to mix all species regardless of mass. We can get away with a single solution to this equation, using only the scale height for atomic sodium, only if atomic sodium is the major species whenever molecular diffusion predominates. Although this turns out to be true for the sodium model presented here, it can be verified only in retrospect.

If we multiply Eq(10) by the concentration of NaX, n_1, we obtain a very convenient differential equation for n_1,

$$\frac{dn_1}{dh} = -\frac{D_{12}}{(D_{12}+K)}\left[\frac{1}{H_1} + (1+\alpha_T)\frac{1}{T}\frac{dT}{dh}\right]n_1 - \frac{K}{(D_{12}+K)}\left[\frac{1}{H} + \frac{1}{T}\frac{dT}{dh}\right]n_1 - \frac{F(h)}{(D_{12}+K)} \tag{12}$$

where F is the downward flux function, obtained by equating

$$F(h) = n_1 w \tag{13}$$

Eq(12) is instructive since the terms in [...] are really just scale heights which contribute to dn_1/dh in relative proportion to the relative magnitudes of the Molecular and Eddy diffusion coefficients at a given altitude. In the molecular diffusion regime, the scale height is that of the independent species, while in the turbulent regime, the scale height is the same as that of the general atmosphere.

Another notable aspect about Eq(12) is the fact that, should q(h) go to zero, as it does at low altitudes, the concentration n_1 still increases since F(h) goes to a constant. This is a result of the increasing number of collisions with decreasing altitude, which must reduce the transport velocity even in the absence of temperature or concentration gradients. Finally, we note that, except for the possible thermal gradient term, which we will see is relatively small by comparison, the concentration n_1 is always increasing with decreasing altitude according to Eq(12).

We have adopted a diffusion coefficient that is similar to that of argon in air, as reported by *Banks and Kockarts* [1973]. It is parameterized by

$$D_{12} = \frac{A T^s}{n} \tag{14}$$

with A equal to 5.5(16) and the exponent s equal to 0.841. The number density of the atmosphere, n, is calculated from the model mass density shown in Figure 1 and the altitude dependent molecular weight, as tabulated by *Kelley* [1989]. Figure 10 shows the average molecular weight of the atmosphere. Figure 11 shows the atmospheric temperature, modeled from the same source.

Around and below 100 km altitude, turbulent mixing of the atmosphere results in a single scale height for all species. This is strictly true in the absence of chemical reactions, the rates for which are large compared to the eddy diffusion time. For this model, the eddy diffusion coefficient was modeled after one given by *Thomas, et al.* [1983]. As can be seen in Eq(12), the diffusion problem depends only on the relative magnitudes of the molecular and eddy diffusion coefficients, D_{12} and K, and on the sum of the two, compared to the total downward flux. Figure 12 shows the relative magnitudes, and Figure 13 shows the sum of the two. Figure 11 is limited to the range of 60 to 120 km, since molecular diffusion dominates completely above 120 km, and eddy diffusion dominates below 60 km. This region is also the region of interest for the chemical model, which will constitute the last step of the modeling effort. It is important, then, that both molecular and eddy diffusion be considered, since the bulk of the sodium present between 90 and 100 km comes from above, where molecular diffusion dominates. Since sodium is, in general, lighter than atmospheric constituents, it is necessary as well to include eddy diffusion to ensure a net downward flux of sodium. With molecular diffusion alone, the net scale height of the sodium would become greater than that of the bulk atmosphere.

The atmospheric scale height of the bulk atmosphere, H, is given by

$$H = 0.8711\, T/m \tag{15}$$

with H in km, T in °K and m in AMU. Profiles for T and m have already been presented. The thermal diffusion term is calculated by numerical differencing of the temperature profile. The thermal diffusion factor α_T is taken to be 0.1, about that for Argon in air. This value is not critical to the calculation in any case.

It is instructive to examine the relative importance of the terms in Eq(10) at various altitudes. To do so, we solve the equation in three ways. First, we use only the source term. We then include the gravitational terms involving the scale heights. Finally, we solve the full diffusion model by including the concentration gradients. Figure 14 shows the three solutions for the initial particle velocity 14 km/s. The region shown is from 50 to 200 km altitude, where the NaX density has become significant. By 200 km, we see that the density of solutions 2 and 3 have tripled over that of solution 1. Solution 1, with the source term alone, represents

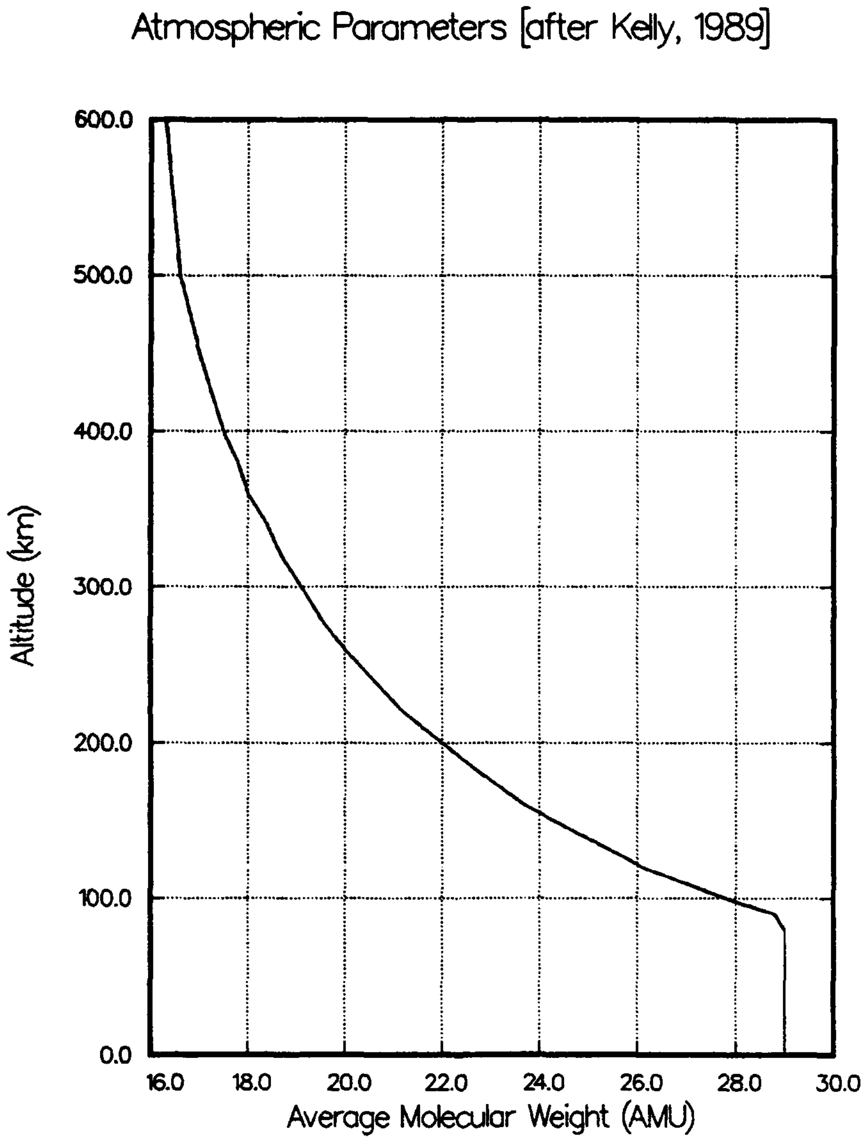

Figure 10. The average molecular weight of the atmosphere [modeled after *Kelley*, 1989].

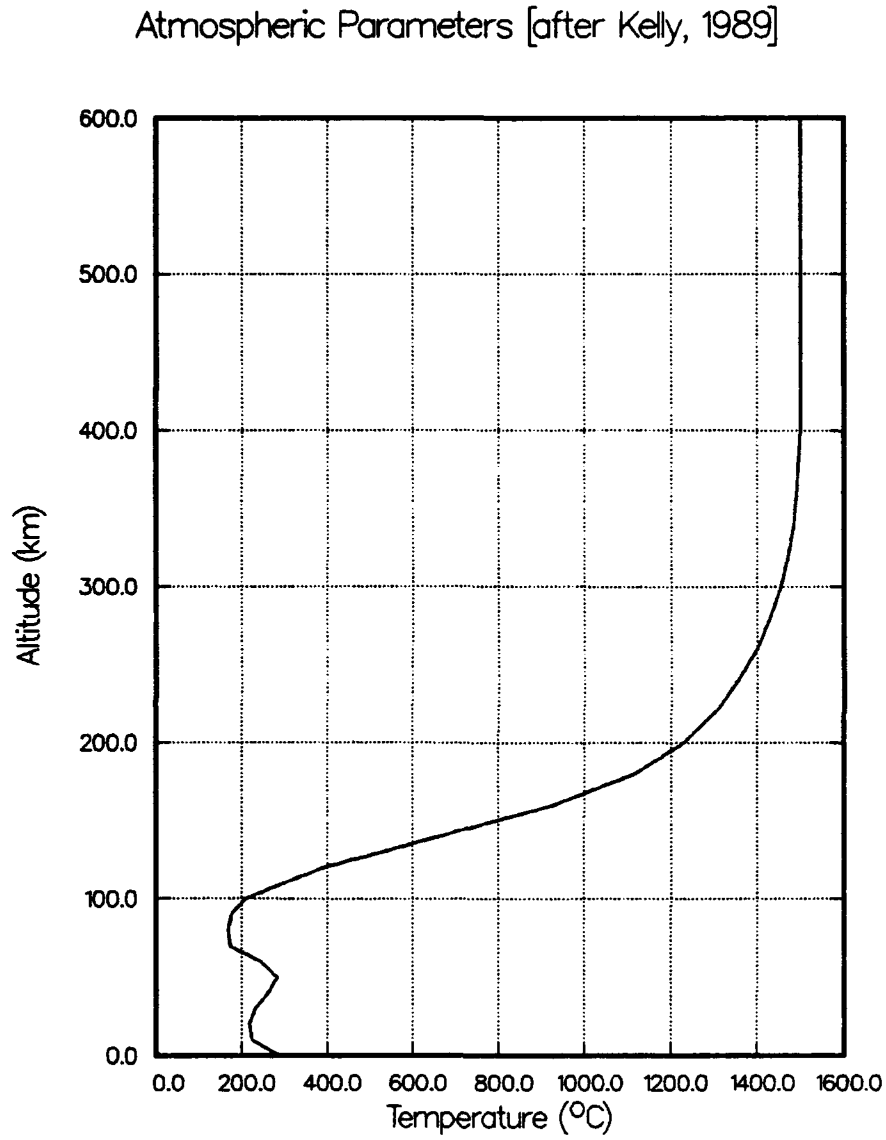

Figure 11. The atmospheric temperature, in °C [after *Kelley*, 1989].

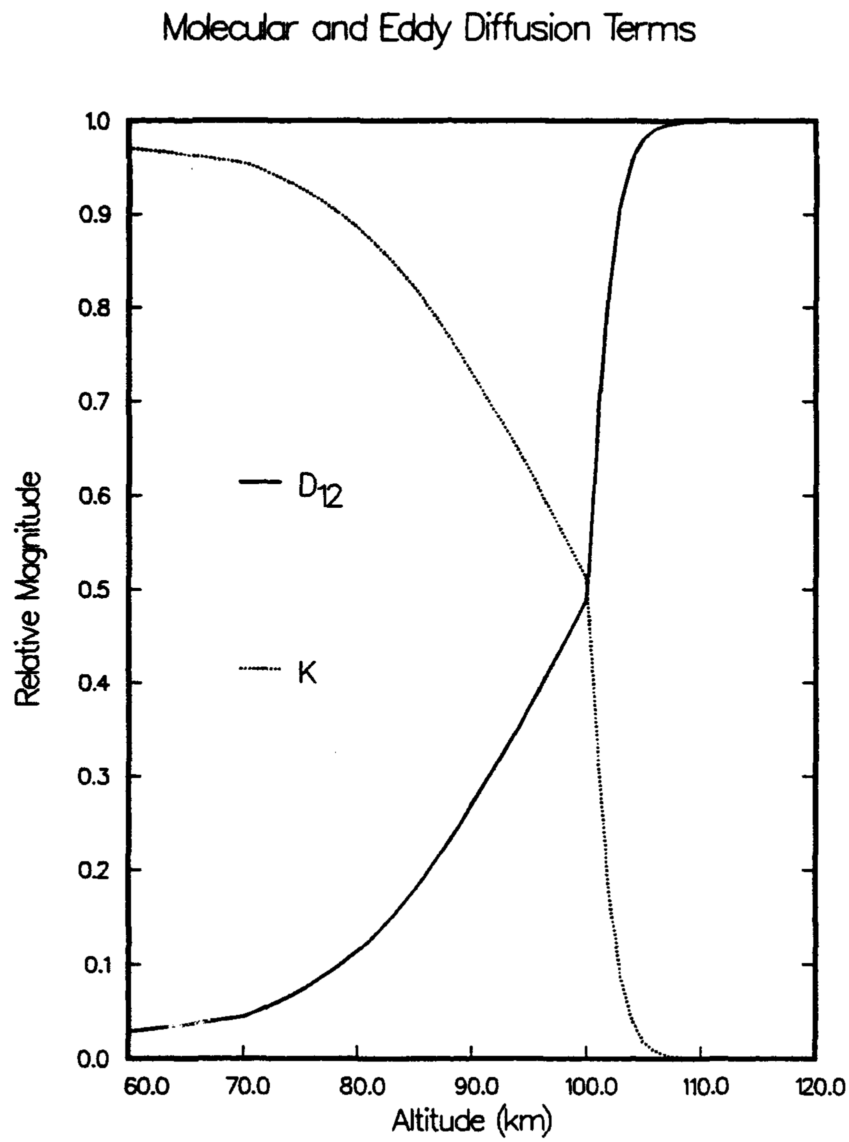

Figure 12. **The relative magnitudes of the eddy and molecular diffusion coefficients.**

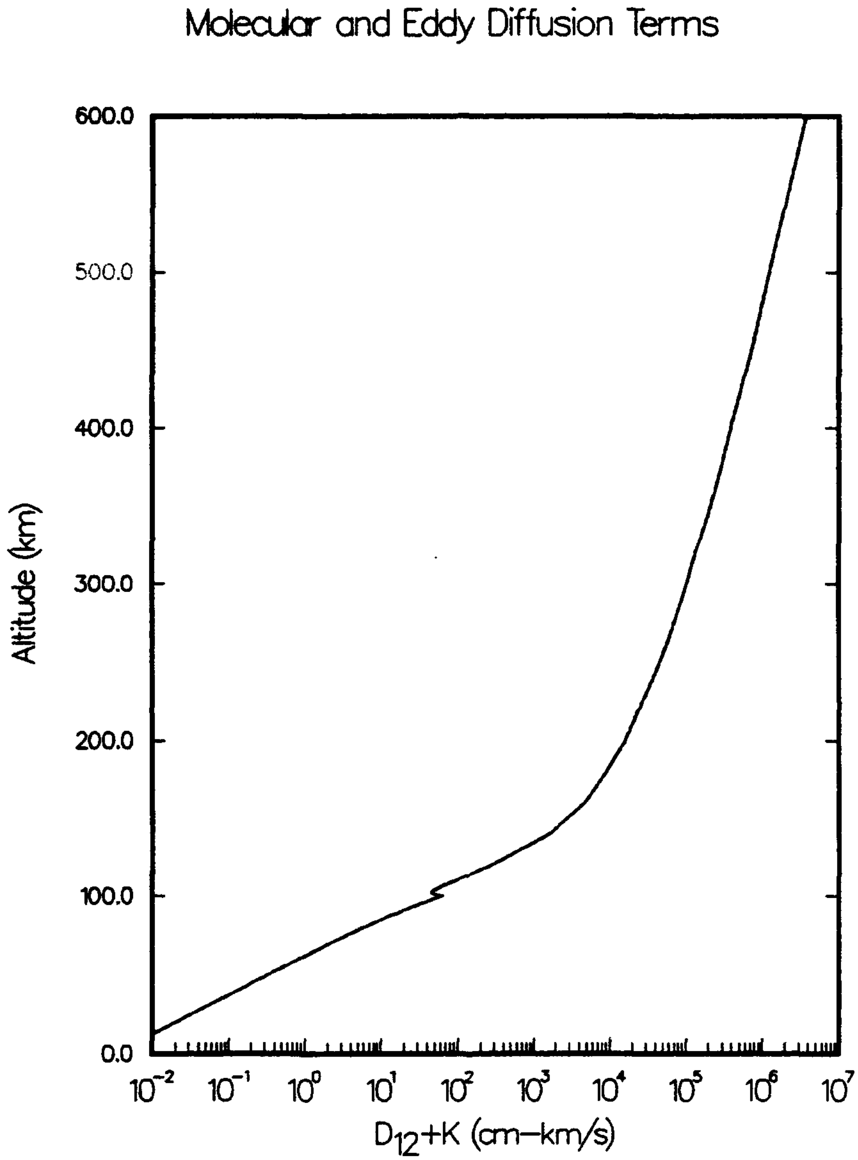

Figure 13. The sum of the eddy and molecular diffusion coefficients as a function of altitude.

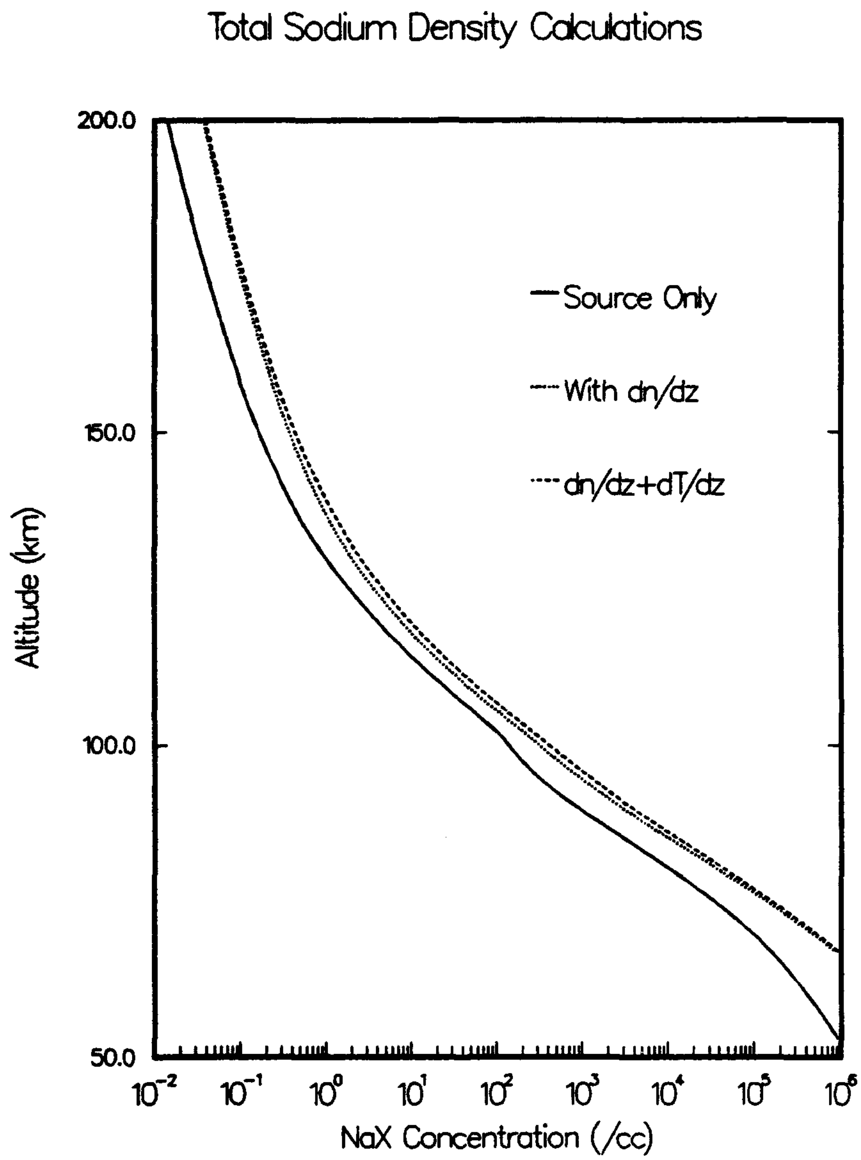

Figure 14. Steady state NaX concentrations, resulting fromo solution of Eq (10) with various terms included (see text).

something of a free molecular motion where the NaX is not influenced by its own concentration gradients. The solution with temperature gradients is quite similar to that without throughout the altitude range. It is at most 20% higher between about 100 and 200 km, where the temperature variation is greatest. The density is more or less exponential, reaching about 3(2)/cc at 100 km and 5(3) at 90 km, the expected peak of the sodium layer.

Another way to look at this solution is to compare the calculated density with the total atmospheric density. This is done in Figure 15. We see that the mixing ratio is shaped more or less like the flux function in Figure 9. The self-consistency of the calculation is evident in that the mixing ratio becomes constant below the region of deposition. This means that the NaX distribution has adapted the scale height of the general atmosphere, and the source term in Eq(12) has become insignificant by comparison. The "roughness" in the low altitude region of Figure 15 is a result of the very large densities there and the discreetness of the total atmosphere model. We do not know if 1(-10) is a reasonable mixing ratio for sodium species at ground level, but at least it does not seem excessively large. We also note that there are heterogeneous removal mechanisms in the troposphere which no doubt can remove sodium species far faster than diffusion below 50 km or so.

A third way to examine this solution is to compare the scale height of the sodium to that of the total atmosphere. Figure 16 shows these. At first, with the calculation beginning at 600 km, the scale height is low. It increases until about 350 km, at which point diffusion begins to dominate the creation from ablation. From 350 km to about 80 km, the scale height of sodium decreases along with the total atmosphere scale height. Below 80 km, it adopts approximately the same scale height of the atmosphere, due to eddy diffusion. For this rough comparison, the scale height was computed numerically from successive points by the formula

$$H_1 = \Delta h / \Delta \log n(\Delta h)$$

Since this calculation depends on the step size and the starting altitude, we should check it with various values of step size Δh and start altitude h_0. Table 3 shows a comparison of the result that will turn out to be critical to the kinetic model, the NaX density at 90 km, for various step sizes and initial altitude. In Table 2, NaX densities are in /cm^3, and step size and start altitude in km. Clearly, considering the precision of this model, the integration parameters are adequate.

TABLE 3. NaX Density with Various Integration Parameters

Step Size --->	1 km	0.2 km
h_0 = 600 km	2.655(3)	2.667(3)
h_0 = 500 km	2.652(3)	2.660(3)
h_0 = 400 km	2.642(3)	2.646(3)

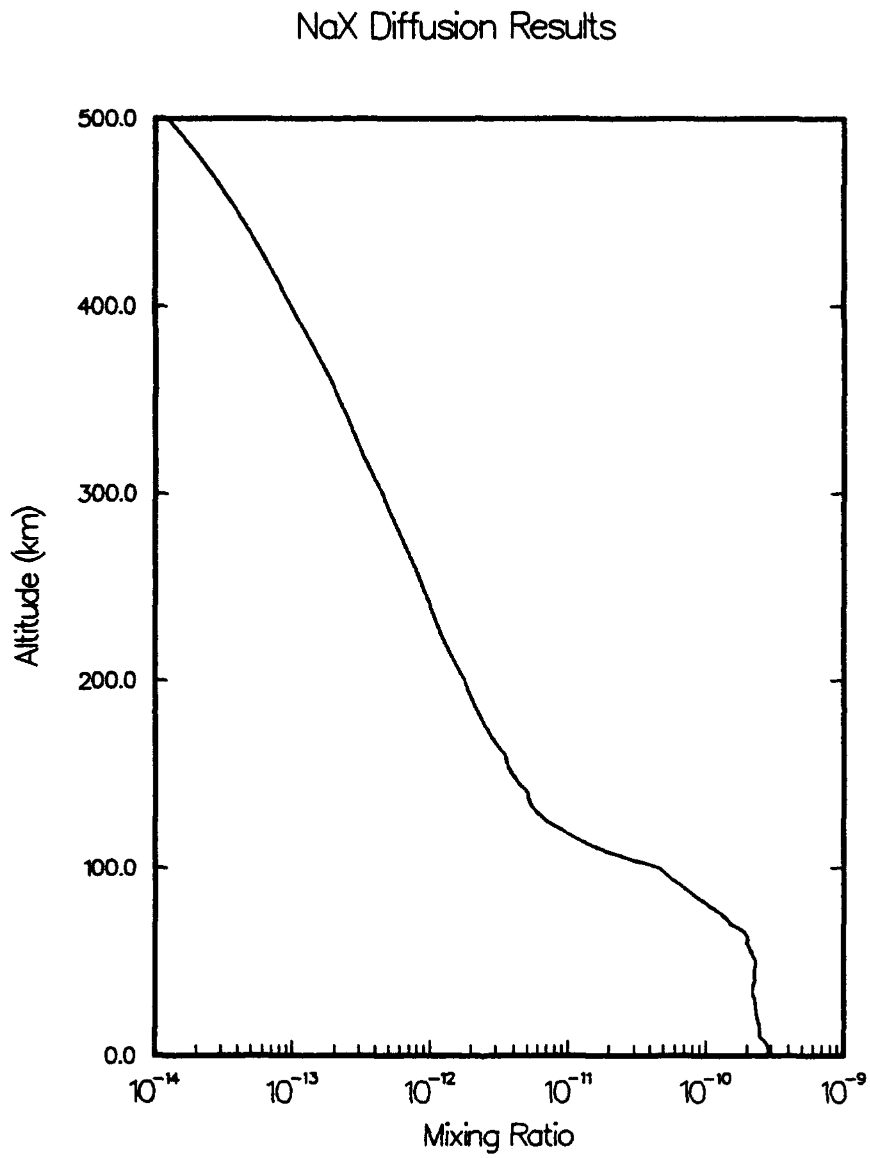

Figure 15. Calculated mixing ratio of total NaX density from solution of the diffusion equation.

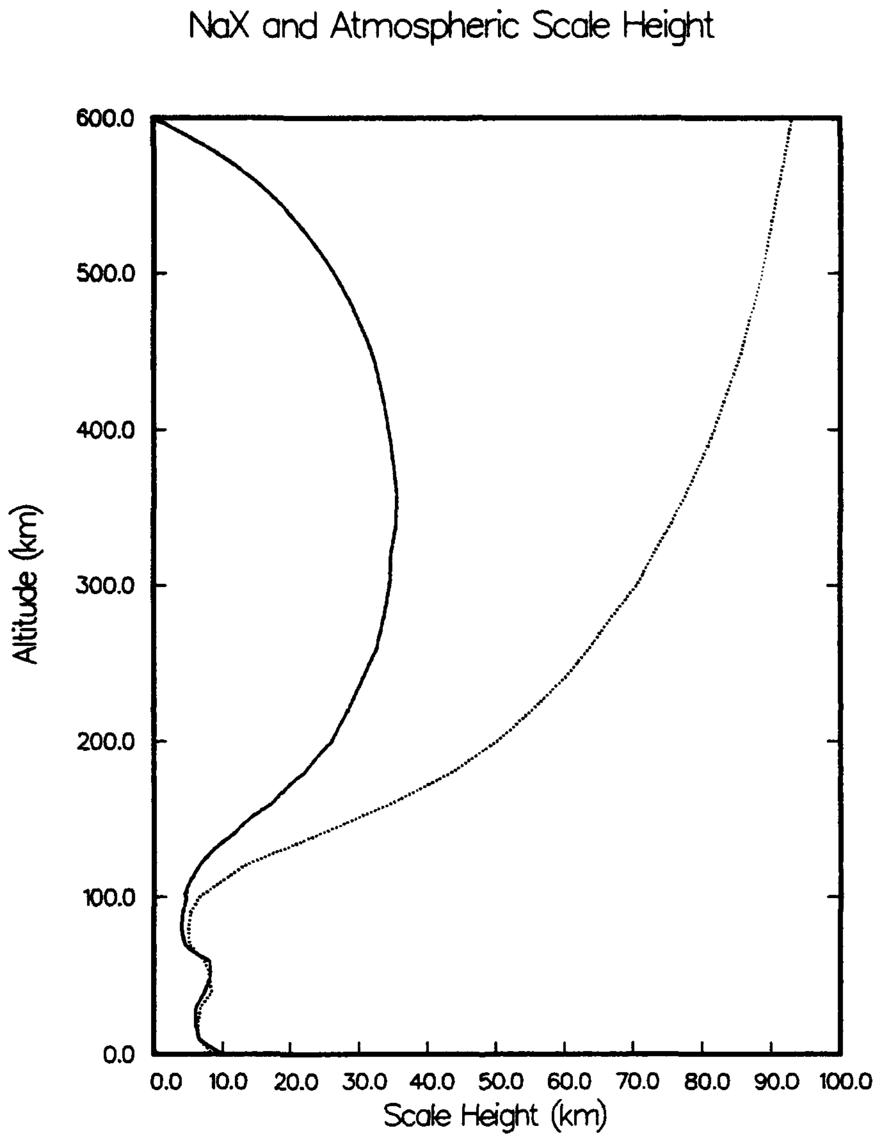

Figure 16. Scale height of calculated NaX density (solid line) and of the total atmosphere.

Having now arrived at a steady state density profile of total sodium species as a function of altitude, we are ready to move on to incorporate the kinetic reactions of sodium with atmospheric constituents.

4.0 THE KINETIC MODEL

The first kinetic model examined is a simplified one, similar to that used by *Swider* [1986] in his study of sodium nightglow. This kinetic model contains only eight reactions between four sodium species and the ambient atoms, but it contains all the essential physics necessary to obtain reasonable estimates of the sodium layer and the nightglow intensity. It is also useful in understanding the general features of the sodium layer because of its relative simplicity. When we move on to a more complicated model, we will see that the results from this simpler one are particularly useful in adjusting the rate constants, since the simpler model is far less sensitive to small rate changes than is the more complex one.

The origin of the 5894Å nightglow was postulated by *Chapman* [1939] as due to the reaction between NaO and O to form atomic sodium, a fraction of which is left in the excited ^2P electronic state.

$$NaO + O \rightarrow Na(^2P, ^2S) + O_2$$

The excited ^2P state would radiate almost immediately to the ground state. Chapman further proposed that NaO would be generated from atomic Na via the reaction

$$Na + O_3 \rightarrow NaO + O_2 ,$$

another mechanism for formation of NaO is the three body reaction

$$Na + O + M \rightarrow NaO + M .$$

But this reaction is of secondary importance in the process, as discovered by *Bates and Ojha* [1980]. *Hussin and Plane* [1982] later suggested a third mechanism involving the reaction

$$Na + O_2 + N_2 \rightarrow NaO_2 + N_2$$

followed by

$$NaO_2 + O \rightarrow NaO + O_2$$

for NaO formation.

The five reactions above would constitute a complete model for the steady state behavior of sodium. However, if we went ahead and solved this model, we would find that the profile of free sodium does not at all resemble a layer, as is found experimentally. What is lacking so far is a reaction to turn sodium into a relatively long lived species at lower altitudes. The complex chain of reactions most likely involves more and more stable species as the reactions progress, but one stable species that can be created directly is NaOH. This is created from NaO by the reaction

$$NaO + H_2O \rightarrow NaOH + OH ,$$

and from NaO_2 by the reaction

$$NaO_2 + OH \rightarrow NaOH + O_2 .$$

These reactions have reasonably well known rate constants. They affect the lower altitude densities of free sodium because both OH and H_2O increase with decreasing altitude. Finally, in order to solve the model, we need to add a 'closure' reaction. If we did not, then the steady state solution would result in 100% NaOH, since NaOH is never returned to any of the other three constituents. A reasonable reaction for this purpose is

$$NaOH + H \rightarrow Na + H_2O .$$

Although the rate of this reaction is not well determined (and in fact, other reactions producing more complex sodium compounds may dominate it), this does not matter, since we will show that the characteristics of the sodium layer and the nightglow are not strongly dependent on this reaction rate. It is necessary only for closure. The reactions, and rate constants as suggested by *Swider* [1986] are given in Table 4.

TABLE 4. Kinetic Model A

#	Reaction	Rate
1	$Na + O_3 \rightarrow NaO + O_2$	7(-10)
2	$NaO + O \rightarrow Na\ (^2P,^2S) + O_2$	1(-10)
3	$Na + O_2 + N_2 \rightarrow NaO_2 + N_2$	2(-30)
4	$NaO + H_2O \rightarrow NaOH + OH$	2(-10)
5	$NaO + O_3 \rightarrow NaO_2 + O_2$	2(-10)
6	$NaO_2 + O \rightarrow NaO + O_2$	1(-13)
7	$NaO_2 + OH \rightarrow NaOH + O_2$	1(-10)
8	$NaOH + H \rightarrow Na + H_2O$	1(-11)

In order to proceed, we must make up altitude dependent models of the major and minor constituents of the ambient atmosphere. To simplify things, we will consider only the region between 60 km and 120 km altitude. Since the steady state problem has now been reduced to a total density for NaX at fixed altitude, the integrations over altitude are complete, and the problem is now solved independently at each altitude. In what follows, we will need concentrations of N_2, O_2, H, OH, H_2O, O, O_3, CO_2, O_2^+, NO^+, and e^-. Although we do not need them all for the present model, we will present them all here for simplicity.

First, we note that we are most interested in calculation of the Na(D) nightglow. Thus, we will restrict the modeling to the night time. For the major atmospheric constituents N_2 and O_2, we assumed perfect mixing below 83 km altitudes, with the U.S. Standard Atmosphere mixing ratios of 78.06% and 20.94%, respectively. Above 83 km, the densities tabulated in the U.S. Standard Atmosphere were used directly. These were interpolated linearly in $\log_{10}n(h)$. Figure 17 shows the result. Minor constituents H, O, and OH were modeled after polynomial fits to discrete points taken from the results of modeling of *Allen, et al.* [1984]. Figure 18 shows these concentrations. For H_2O, the mixing ratio reported by *Allen, et al.* was fit to a polynomial and then multiplied by the total atmospheric density, which was in turn obtained from the model atmosphere in Figure 1 and the average molecular weight in Figure 10. The CO_2 profile was produced by another polynomial fit to the curve presented by *Keneshea, et al.* [1979]. Figure 19 shows these densities.

The ozone density was allowed to vary somewhat in these models, since part of the purpose of the kinetic modeling was to ascertain the effect of varying ozone density on the sodium nightglow. We adapted a general profile reported by *Allen, et al.* [1984] as determined from rocket measurements, but allowed the density to vary by a factor of 10 over that reported. Figure 20 shows the minimum and maximum ozone concentrations considered in this model. For reference, our minimum ozone density at 90 km is about a factor of two less than that of *Sze, et al.* [1982]. Also, *McPeters* [1980] has noted an approximately 10-fold increase in O_3 at 1 mbar (altitude $\sim$ 50 km) from Nimbus-4 BUV measurements, so this range of variability is not especially extreme. Finally, we will need to model charge exchange and molecular dissociative recombination, for which we take NO^+, O_2^+, and e^- densities from the International Reference Ionosphere (IRI) at conditions for January at midnight at the equator. These are shown in Figure 21.

To solve this model, and all subsequent ones, a file is prepared containing all reactions and rate constants to be considered. We have written a software program called KINO which reads this file and, from it, prepares a subroutine through which the equations are solved. This prevents errors in coding, which can become quite complicated as the number of reactions and constituents increase. The system of equations is then solved in the steady state. The details of the KINO routine and of the steady state solution are given in the appendix.

The steady state solution to Model A is shown in Figure 22. The kinetics has produced a well defined free sodium layer, centered around about 88 km altitude. Below this, there is a substantial concentration of both NaO_2 and NaOH. At even lower altitudes, the NaO_2 has given

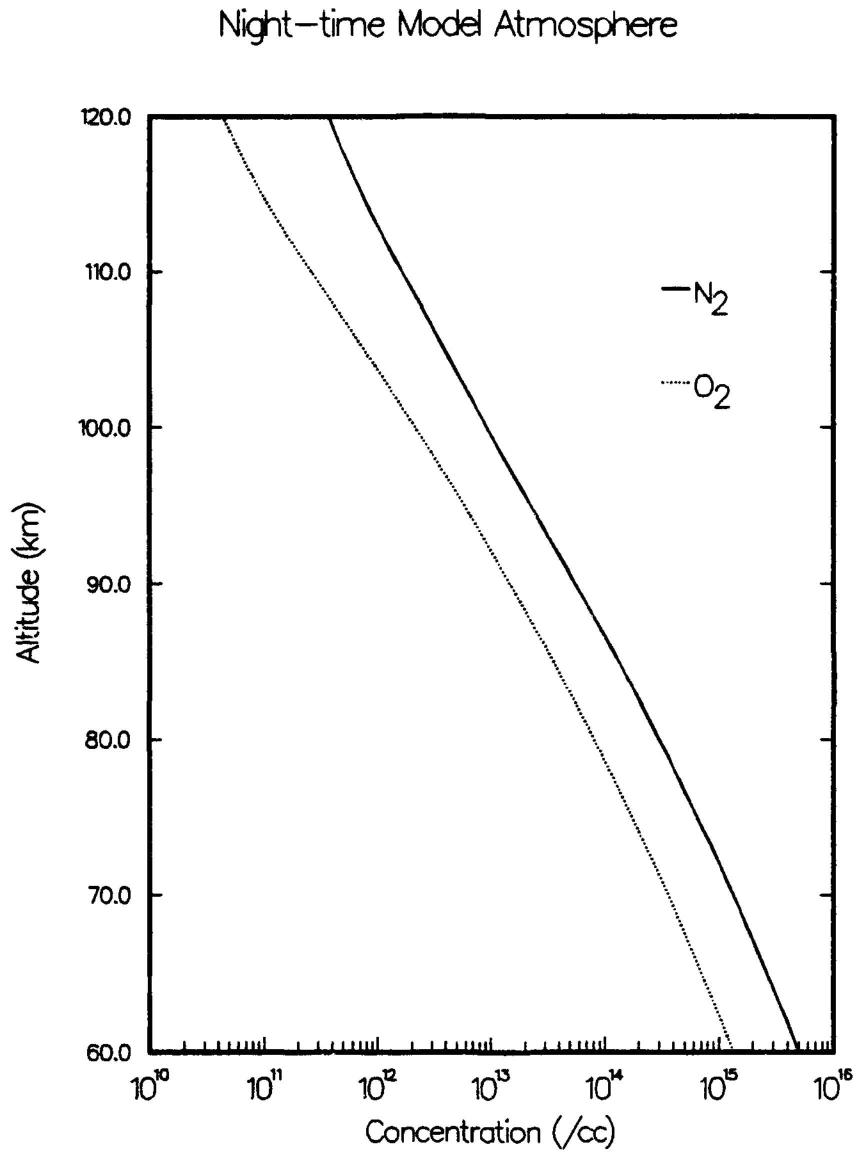

Figure 17. N_2 and O_2 density as a function of altitude for the night-time model atmosphere.

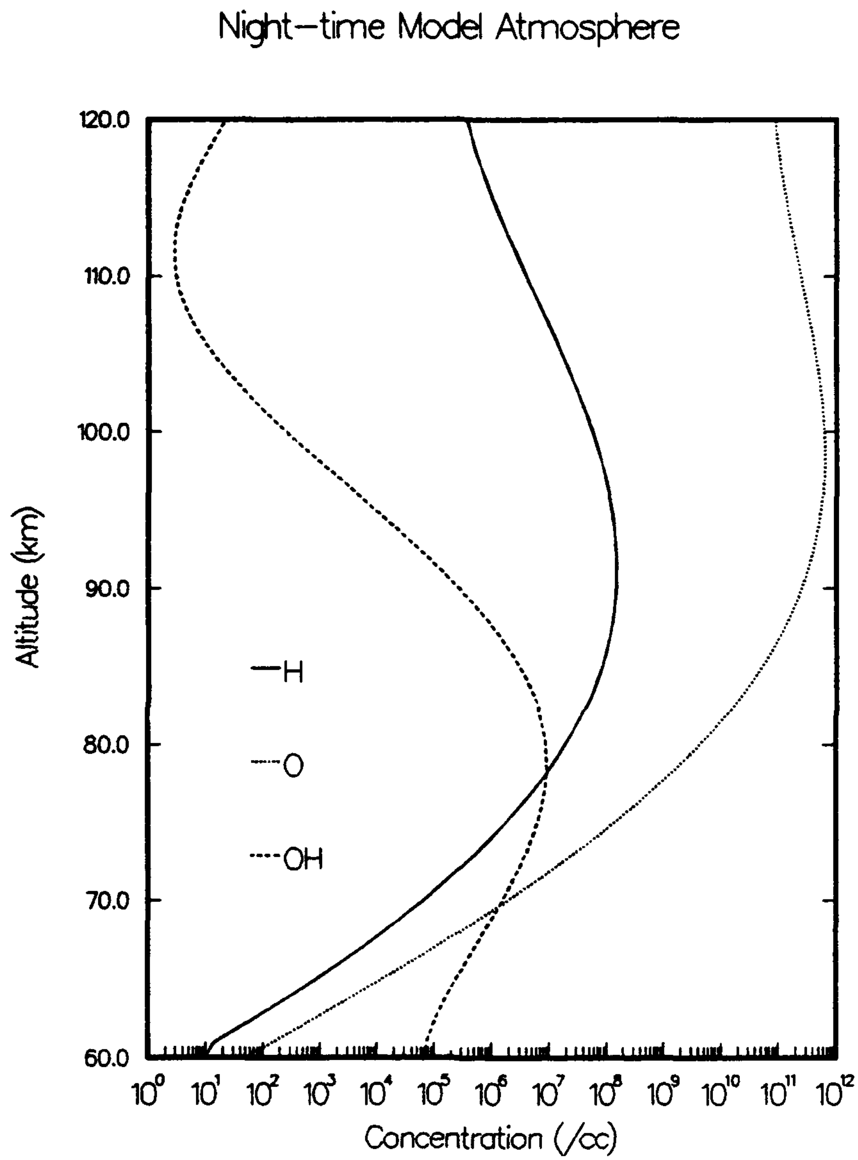

Figure 18. O, H, and OH density as a function of altitude for the night-time model atmosphere.

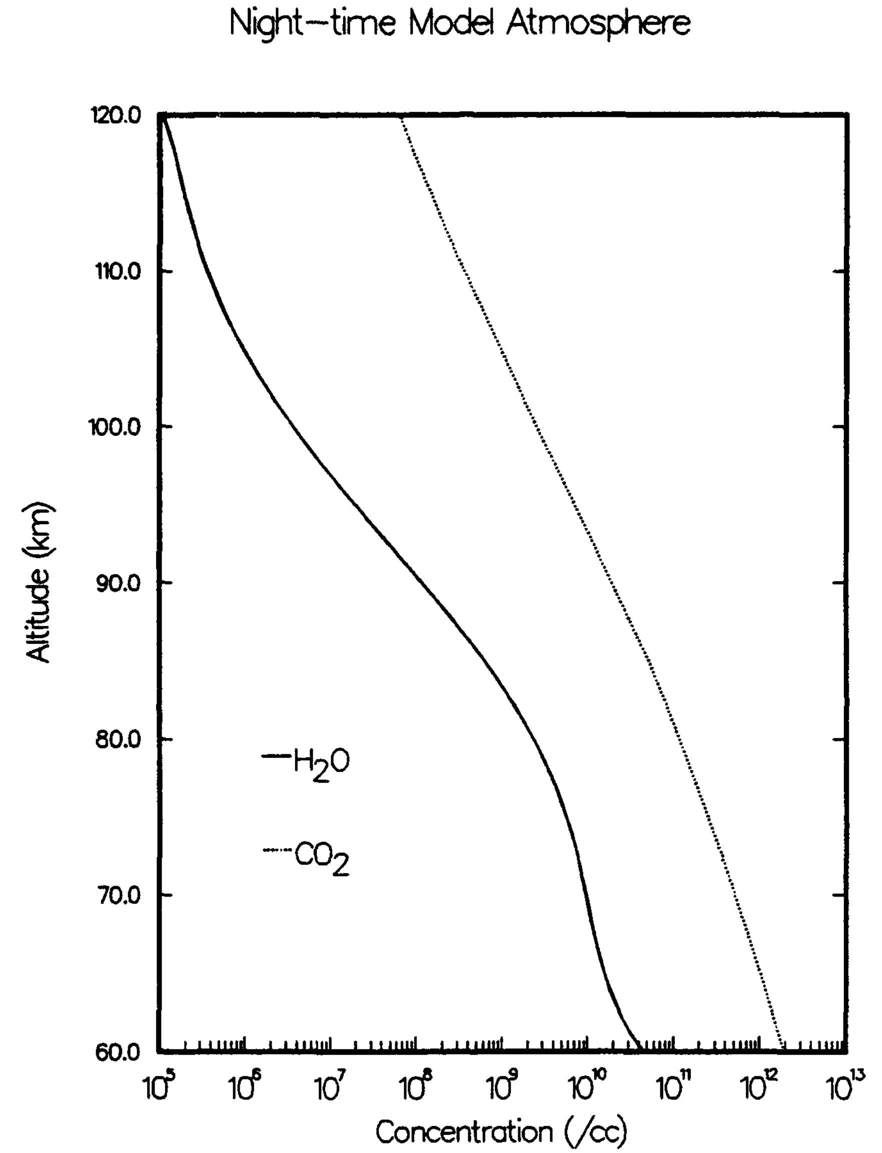

Figure 19. H_2O and CO_2 density as a function of altitude for the night-time model atmosphere.

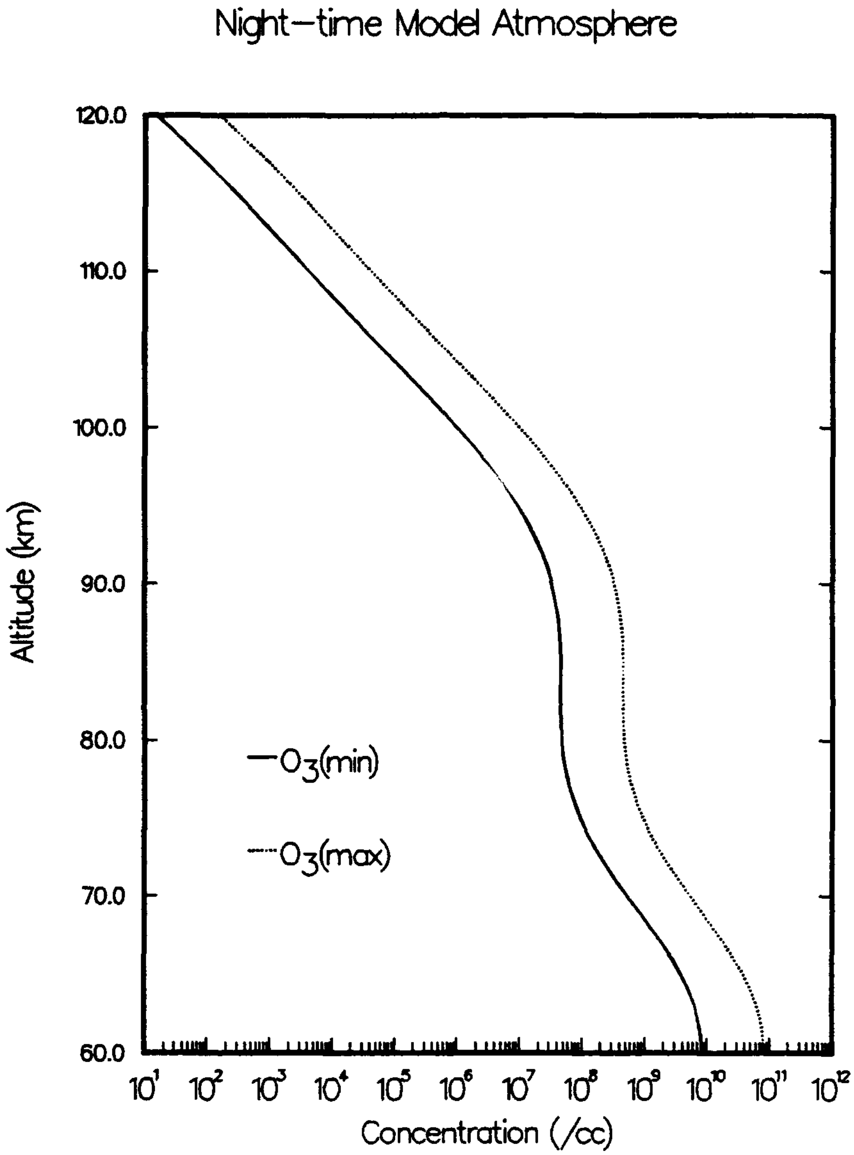

Figure 20. **Minimum and maximum modeled O_3 density as a function of altitude for the night-time model atmosphere.**

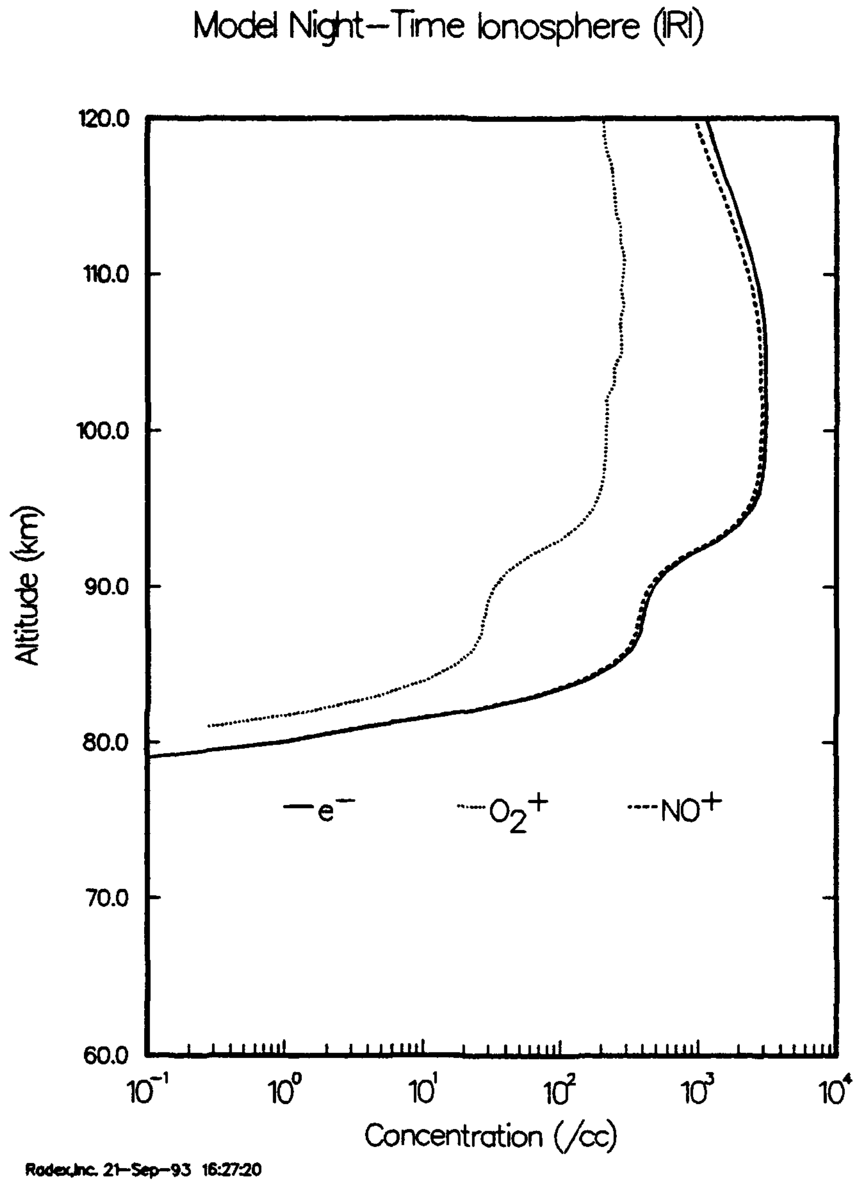

Figure 21. Model ionosphere (IRI at midnight, equator, January) as a function of altitude.

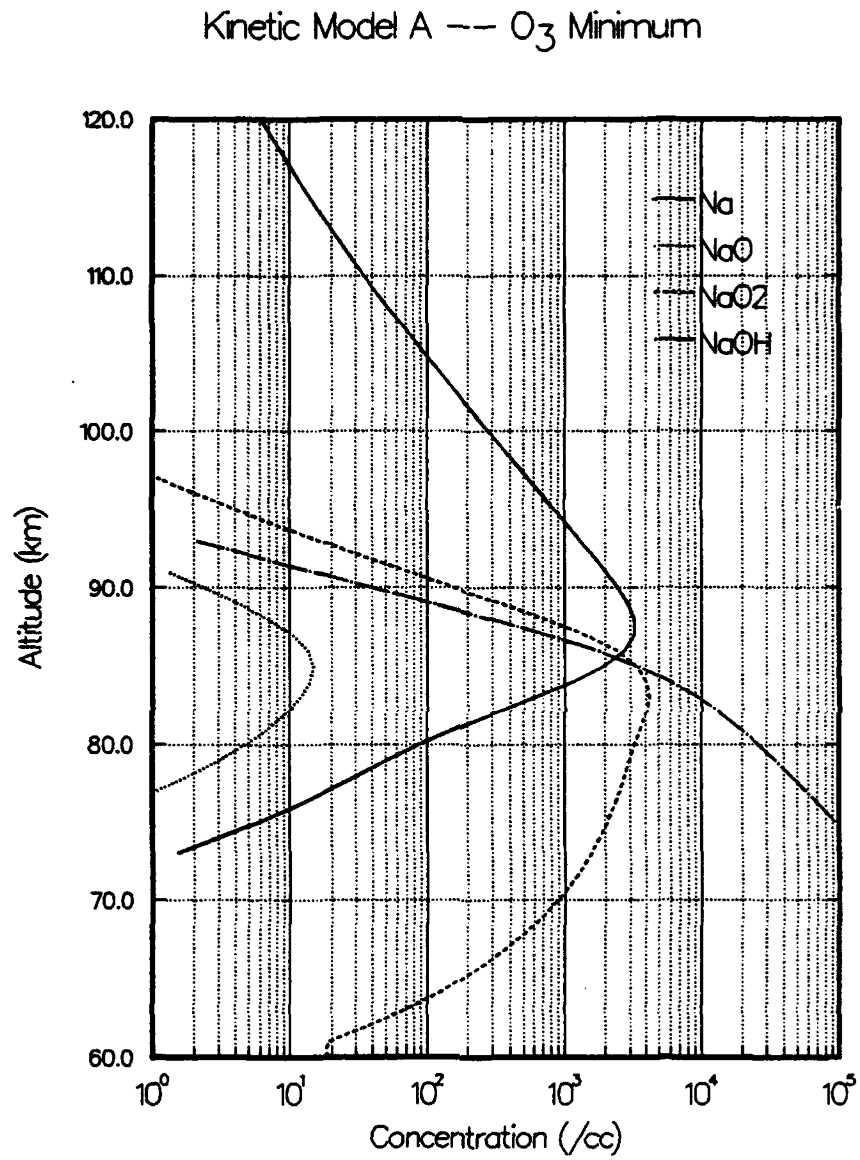

Figure 22. The concentration of sodium species resulting from solution of Kinetic Model A, run with initial meteor velocity of 14 km/s and ozone concentration at minimum.

way in favor of NaOH completely. The reason that there is a layer of free sodium is that atomic oxygen rapidly converts NaO back to free sodium and atomic hydrogen NaOH to Na at these altitudes. As the concentration of O and H drops off below 85 km or so, these reactions no longer dominate. NaOH becomes the major product at low altitudes because it is destroyed only by the reaction with H, which trails off even more rapidly than O or OH, according to Figure 18. NaOH is the major low altitude species in this model only because no further reactions have been specified which could convert it into more complex species, $NaHCO_3$ for example. Even with its simplicity, though, the model has reproduced the sodium layer well, in agreement with experimental evidence. *Tilgner and von Zahn* [1988], for example, have calculated the mean sodium layer at 64° north in winter from lidar measurements. Their result shows a peak height of around 88 km and a peak magnitude of from 3(3) to 4(3) particles/cm^3. Model A, as evaluated here with an initial particle velocity of 14 km/s, gives a peak height at about 87 km with magnitude of 3.3(3) particles/cm^3.

Here, we investigate the behavior of the model as a function of particle velocity. As we recall, the initial velocity of the particle was held fixed in the Monte Carlo calculation of deposition. This was mainly because no data was available on the precise distribution of these velocities. *Hughes* [1991] states that a reasonable range for the vast majority of particles is 13.8 to 16.2 km/s. In Table 5 we show the various values of the peak intensity of the sodium layer for initial velocities between 12 and 16 km/s. These are shown both for ozone minimum and ozone maximum values. In all cases, the peak height is either 87 or 88 km altitude. As can be seen, the dependence on initial velocity is small, less than 10% in all cases. Interestingly too, the maximum in the sodium layer intensity comes at around 15 km/s. The variation exhibits a maximum because the ablation height falls as velocity increases, however, as the height falls, more Na becomes NaO_2 and NaOH, leading to an overall decrease. On the other side, ablation at higher altitudes increases peak density.

TABLE 5. Variation of Na Layer Maximum (/cc) with Initial Particle Velocity

Velocity (km/s)	Ozone Minimum	Ozone Maximum
12	3.037(3)	2.104(3)
14	3.240(3)	2.244(3)
16	3.226(3)	2.233(3)

Considering now the problem of sodium night-glow, we note that the number of photons per cm^3-s should be proportional to the rate of reaction 2 in this model. This proportionality constant will be the branching ratio between the ^2P and ^2S states. It is well known that about one-third of the Na from reaction 2 ends up in the excited ^2P state, so that the volume emission rate is given by

$$r = \frac{1}{3} k_2 [NaO][O] \tag{16}$$

Figure 23 shows the volume emission rate as a function of altitude for this model at ozone minimum. The night-glow layer peaks at about 35 photons/cm^3-s at a height about equal to the height of the sodium layer, 88 km.

To arrive at a total intensity of Na(D) emission, we simply integrate up the column.

$$I = \int_0^\infty r(h)\,dh \tag{17}$$

which we do by Simpson's rule. Since one Rayleigh is 1(6) photons/cm^2-s and since we use 1-km altitude divisions, the normalization factor is one-tenth. For the case shown in Figure 23, the total intensity is 24.7 R, for ozone minimum. In the case of ozone maximum, the intensity comes out to be 130.2 R, an increase of about 500%. The increase in night-glow with increasing ozone concentration is not directly proportional because, as we can see from Table 5, the increase in ozone causes a decrease in steady state Na density, which in turn drives the emission process. Also, Reaction 3 of Model A, followed by Reaction 6 is also a source of NaO, although a relatively minor one. We can examine this by running the model without any ozone at all. The major effects are the lowering of the night-glow peak to about 85 km and the lowering of the intensity to about 4.1 R. Thus, at ozone minimum, the three-body reaction process contributes about 20% to the total night-glow.

In the process of creating a more comprehensive model of sodium chemistry, we will add reactions to the chain a few at a time. We now introduce Model B, which will add three species. First, we will attempt to reproduce the model of *Plane* [1991], who includes a total of seventeen reactions. These are shown in Table 6. Aside from a few minor changes in rate constants, there are some differences between the reactions in Model A. The reaction of NaO with ozone

$$NaO + O_3 \rightarrow Na + 2O_2$$

has been added as a way to recycle atomic sodium. Also, three-body reactions between NaO and O_2 or CO_2 have been added, and a three-body reaction between NaOH and CO_2, as well. Also of note, the recycling of NaO_2 with OH has been replaced by recycling with H in Model B. The three-body reactions of NaO now form NaO_3 and $NaCO_3$. Both of these are converted back to NaO_2 with atomic oxygen. Finally, $NaCO_3$ is allowed to react with hydrogen, also in a three-body reaction, to form $NaHCO_3$. $NaHCO_3$ is recycled to atomic sodium with atomic hydrogen alone.

$$NaHCO_3 + H \rightarrow Na + H_2CO_3$$

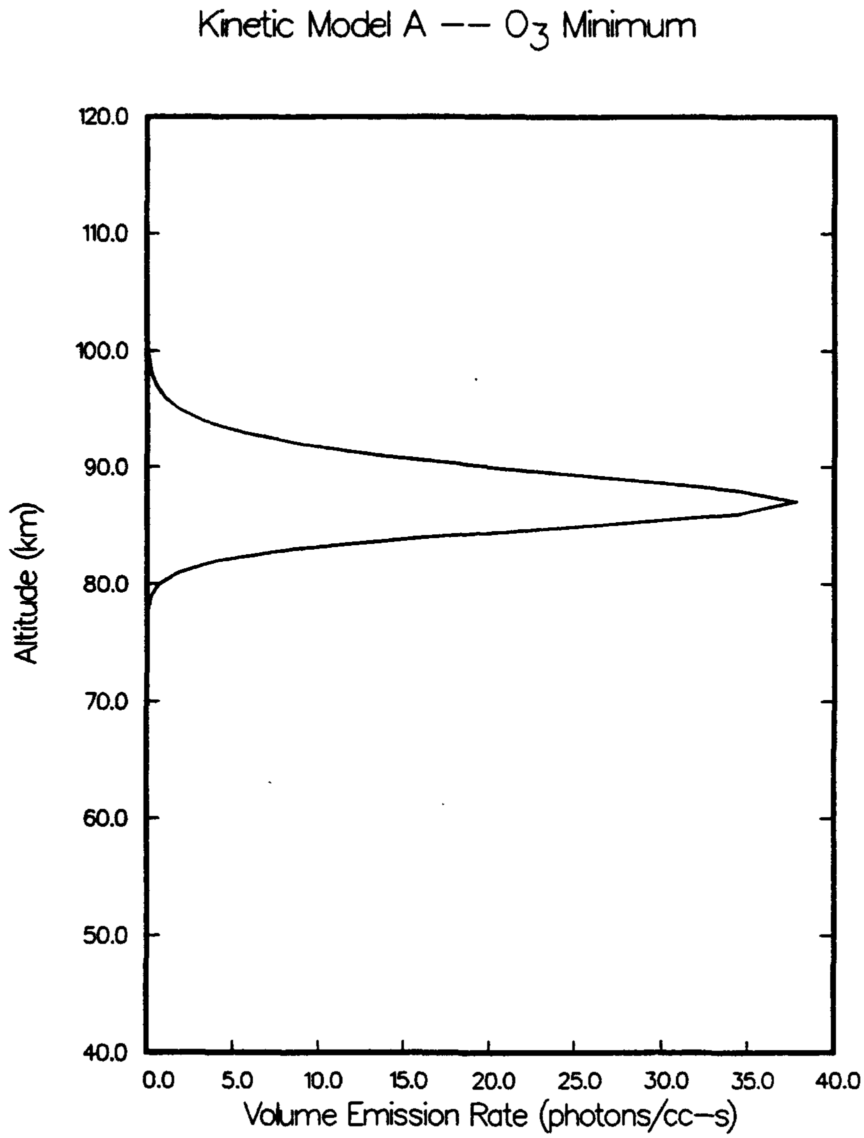

Figure 23. The rate of $Na(^2P)$ emission as a function of altitude, calculated from the solution to Kinetic Model A at O_3 minimum.

We will see that this reaction is especially important in the overall behavior of this model.

Figure 24 shows the sodium species resulting from the solution of Model B. The first striking difference between Model B and Model A is that the peak sodium density in Model B has decreased to 8.2(2)/cm^3. The height of the layer has increased as well to 93 km. At 90 km, the major species is $NaHCO_3$, comprising more than 80% of the total NaX. The intensity of the Na(D) emission has fallen dramatically to only 2.2 R.

TABLE 6. Kinetic Model B

#	Reaction	Rate
1	$Na + O_3 \rightarrow NaO + O_2$	6.0(-10)
2	$NaO + O \rightarrow Na(^2P,^2S) + O_2$	2.2(-10)
3	$NaO + O_3 \rightarrow NaO_2 + O_2$	1.5(-10)
4	$NaO + O_3 \rightarrow Na + 2O_2$	2.0(-11)
5	$NaO + H_2O \rightarrow NaOH + OH$	1.8(-10)
6	$NaO + O_2 + N_2 \rightarrow NaO_3 + N_2$	5.3(-30)
7	$NaO + CO_2 + N_2 \rightarrow NaCO_3 + N_2$	1.3(-27)
8	$Na + O_2 + N_2 \rightarrow NaO_2 + N_2$	4.7(-30)
9	$NaO_2 + O \rightarrow NaO + O_2$	2.0(-14)
10	$NaO_2 + H \rightarrow NaOH + O$	1.9(-14)
11	$NaOH + H \rightarrow Na + H_2O$	4.0(-13)
12	$NaOH + CO_2 + N_2 \rightarrow NaHCO_3$	1.9(-28)
13	$NaO_3 + O \rightarrow Na + 2O_2$	2.0(-14)
14	$NaO_3 + O \rightarrow NaO_2 + O_2$	2.0(-14)
15	$NaCO_3 + O \rightarrow NaO_2 + CO_2$	1.0(-13)
16	$NaCO_3 + H + N_2 \rightarrow NaHCO_3 + N_2$	1.0(-30)
17	$NaHCO_3 + H \rightarrow Na + H_2CO_3$	1.0(-14)

Comparing these results to those of Plane, we find that the peak height agrees quite well. However, he obtains a peak density of about 3(3)/cm^3 and, more importantly, the sodium at the peak is almost entirely in the atomic form. His peak NaO density is approximately 10/cm^3, leading to an integrated intensity of 106 R, as reported there. Finally, the model evaluated with

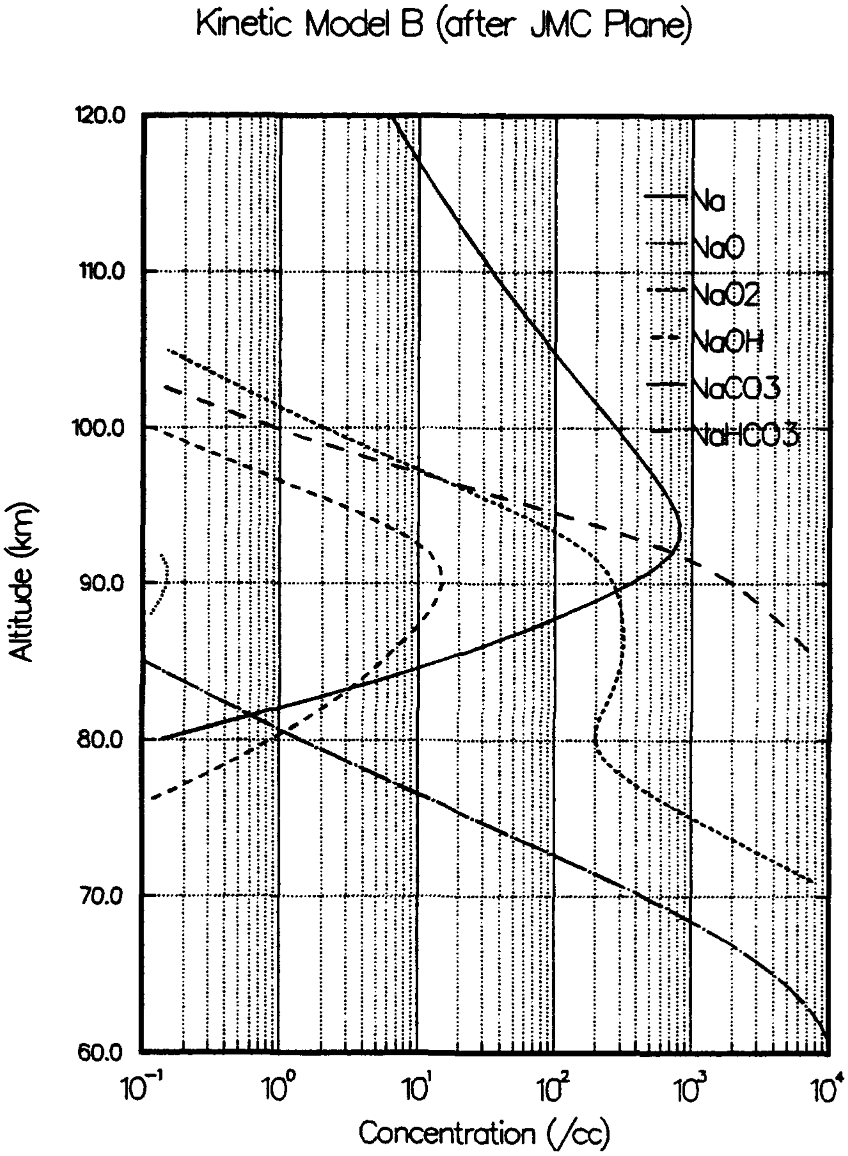

Figure 24. The concentration of sodium species resulting from the solution of Kinetic Model B.

our atmosphere shows that the major constituent below the sodium layer is $NaHCO_3$. However, the figure in Plane seems to indicate that NaO_2 is the major species. We believe that there must be some dramatic difference in our atmospheric model from that used by Plane. This is somewhat difficult to verify, since the atmosphere used by Plane is not explicitly specified.

It is instructive to examine the effects of variations of certain key rate constants in the model, in order to ascertain the reasons for the possible discrepancies. First, we note that reaction 9, between NaO_2 and O is a factor of five smaller in Model B than in Model A. We try increasing it by a factor of five. The effect is shown in Table 7. This reaction increases the peak density and radiance only slightly. Next, we examine the "closure" reactions, for which the rates are very speculative for lack of measurements. Increasing Reaction 15 and Reaction 16 rates by factors of 100 has almost no effect. However, increasing the rate at which $NaHCO_3$ is converted back to Na increases the peak density to almost what it was in Model A. Importantly, also, we see that after the rate is increased 1,000 times, further increases, even by a factor of 10, do not significantly change the results. This is as it should be, indicating that atomic Na is the major species in the lower thermosphere.

TABLE 7. Effects of Variation of Rates in Model B

Variation	Na Peak (/cc)	Peak Altitude (km)	Night-glow (R)
Original Model	818	93	2.4
Reaction 9 increased by a factor of 5	959	93	2.8
Reaction 15 increased by a factor of 100	959	93	2.8
Reaction 16 increased by a factor of 100	959	93	2.8
Reaction 17 increased by a factor of 100	2313	89	16.3
Reaction 17 increased by a factor of 1,000	2588	88	22.2
Reaction 17 increased by a factor of 10,000	2630	88	23.5

We cannot determine precisely why the Plane kinetic model does not produce results in good agreement with the simpler Model A. However, the adjustment of the closure rates does bring the results close in line with both the simpler model and with expected results based on observation.

TABLE 8. Kinetic Model C

#	Reaction	Rate Model B	Rate Model C
1	$Na + O_3 \rightarrow NaO + O_2$	6.0(-10)	7.0(-10)
2	$NaO + O \rightarrow Na + O_2$	2.2(-10)	1.0(-10)
3	$NaO + O_3 \rightarrow NaO_2 + O_2$	1.5(-10)	2.0(-10)
4	$NaO + O_3 \rightarrow Na + 2O_2$	2.0(-11)	2.0(-11)
5	$NaO + H_2O \rightarrow NaOH + OH$	1.8(-10)	2.0(-10)
6	$NaO + O_2 + N_2 \rightarrow NaO_3 + N_2$	5.3(-30)	5.3(-30)
7	$NaO + CO_2 + N_2 \rightarrow NaCO_3 + N_2$	1.3(-27)	1.3(-27)
8	$Na + O_2 + N_2 \rightarrow NaO_2 + N_2$	4.7(-30)	2.0(-30)
9	$NaO_2 + O \rightarrow NaO + O_2$	2.0(-14)	1.0(-13)
10	$NaO_2 + H \rightarrow NaOH + O$	1.9(-14)	1.9(-14)
11	$NaOH + H \rightarrow Na + H_2O$	4.0(-13)	1.0(-11)
12	$NaOH + CO_2 + N_2 \rightarrow NaHCO_3$	1.9(-28)	1.9(-28)
13	$NaO_2 + OH \rightarrow NaOH + O_2$	--	1.0(-10)
14	$NaO_3 + O \rightarrow Na + 2O_2$	2.0(-14)	2.0(-14)
15	$NaO_3 + O \rightarrow NaO_2 + O_2$	2.0(-14)	2.0(-14)
16	$NaCO_3 + O \rightarrow NaO_2 + CO_2$	1.0(-13)	1.0(-11)
17	$NaCO_3 + H + N_2 \rightarrow NaHCO_3 + N_2$	1.0(-30)	1.0(-28)
18	$NaHCO_3 + H \rightarrow Na + H_2CO_3$	1.0(-14)	1.0(-11)

We make a few more minor modifications to this model to arrive at Model C, which is shown in Table 8. The modifications include rate constant modifications to conform better to Model A, and the re-introduction of the reaction

$$NaO_2 + OH \rightarrow NaOH + O_2 ,$$

which was in Model A but not in Model B. For comparison, Table VIII also shows the rate constants from Model B alongside. The results for the constituents from the solution of Kinetic Model C are shown in Figure 25. Notably, $NaHCO_3$ remains the predominant species below the sodium layer. NaO, which is responsible for the sodium nightglow, has come back up to a level of about 10/cc at an altitude of 85 km.

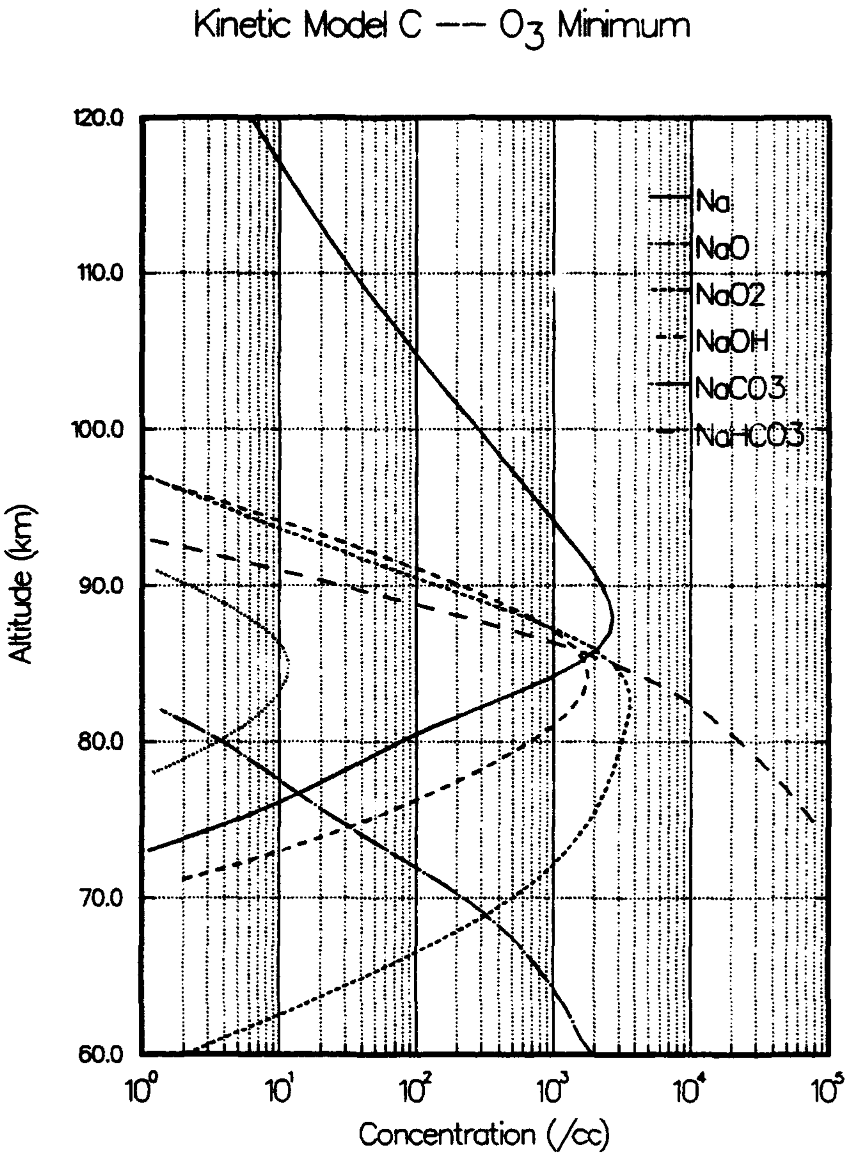

Figure 25. The concentration of sodium species resulting from the solution of Kinetic Model C.

In the next step, we examine further what might happen to the primary low altitude product $NaHCO_3$. NaO_2 reacts with O, H, and OH at high altitudes. However, at lower altitudes there is very little of these three species present. There, the primary reaction is probably the three-body reaction

$$NaO_2 + CO_2 + N_2 \rightarrow NaCO_3 + O + N_2 \,,$$

and $NaCO_3$ can react further through another three-body reaction

$$NaCO_3 + Na + N_2 \rightarrow Na_2CO_3 + N_2 \,.$$

Eventually, the Na_2CO_3 would form complex crystals and fall from the atmosphere. However, the modeling of this is somewhat complex and we will terminate the chain of reactions here. In order to solve this model, however, we need a closure reaction, which we choose to be

$$Na_2CO_3 + O \rightarrow NaCO_3 + NaO$$

Choosing rate constants of 1.0(-30), 1.0(-28), and 1.0(-16) for these three new reactions respectively, gives the results for our Kinetic Model D, shown in Figure 26. Although the results above about 80 km have not changed at all as a result of the addition of the three-body reactions, we see that the low altitude model is quite different. The $NaHCO_3$ has formed a layer with a maximum of about 1(5)/cc at around 70 km. Below this, the major component is $NaCO_3$ for a short time, giving way at lower altitudes to Na_2CO_3. Increasing the rate of the second of the new reactions in relation to the first would no doubt reduce the $NaCO_3$. However, without either accurate measurements of the rates or experimental observations of these species, this would be a rather speculative exercise.

Finally, we finish out the model by adding the ionic reactions. These include charge exchange of atomic Na with both O_2^+ and NO^+,

$$Na + O_2^+ \rightarrow Na^+ + O_2$$

and

$$Na + NO^+ \rightarrow Na^+ + NO \,.$$

The sodium ion is then assumed to react with two N_2 atoms to form the relatively stable complex NaN_2^+

$$Na^+ + N_2 + N_2 \rightarrow NaN_2^+ + N_2 \,.$$

Finally, molecular dissociative recombination (MDR) can take place to close out this cycle.

$$NaN_2^+ + e^- \rightarrow Na + N_2$$

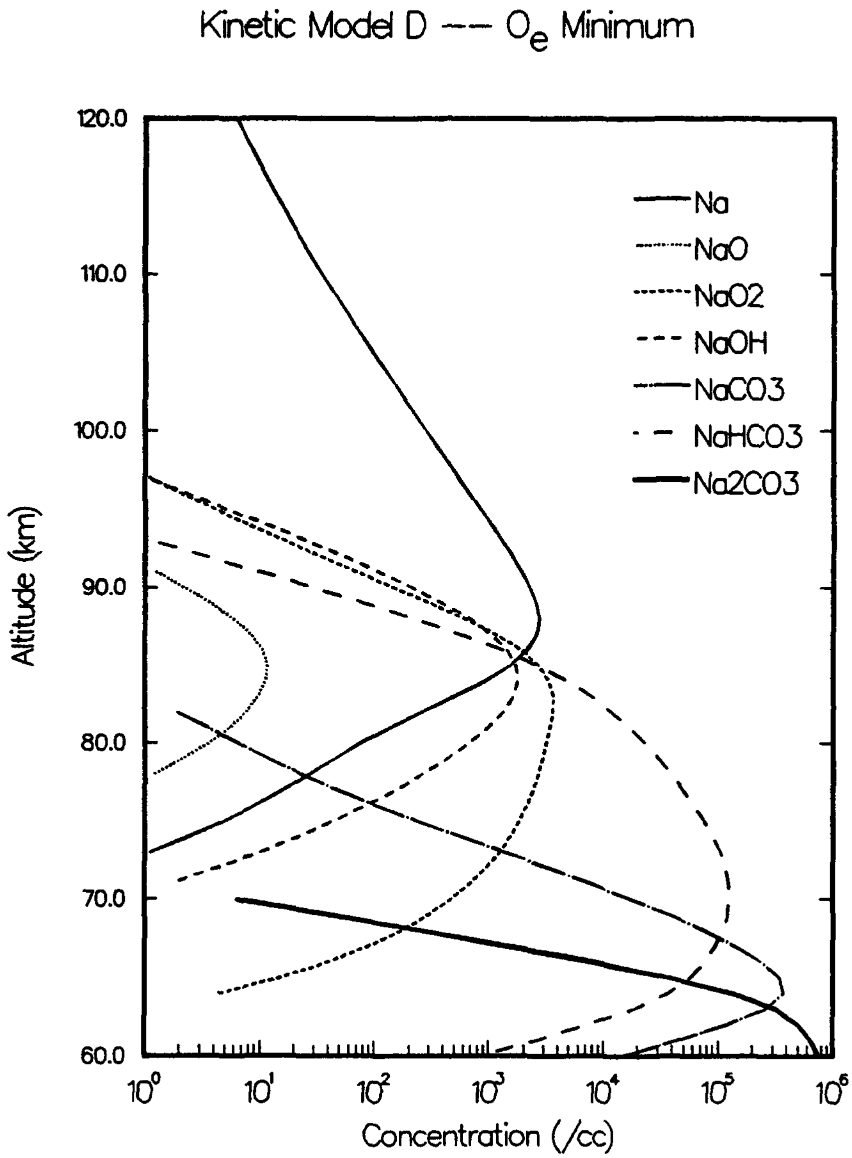

Figure 26. **The concentrations of sodium neutral compounds resulting from the solution of Kinetic Model D.**

The final model is shown along with all rate constants in Table 9. This is the model which will be used for the remainder of the work and is called Kinetic Model E.

The neutral atomic sodium and the ions from Model E are shown in Figure 27. Sodium ion dominates above an altitude of about 105 km. NaN_2^+ begins to form as the total atmospheric density becomes substantial and mirrors the decrease in atomic sodium with decreasing altitude. Figure 28 shows the sodium compounds resulting from Model E. Except for a decrease in the top-side atomic sodium density, the results are almost identical to Model D. Figure 29 shows the variation of sodium night-glow with ozone density. Here, the ozone density was varied by multiplication by the factor α_{O3}.

The $\alpha=0$ limit has been included in the data in Figure 29 to show the importance of the reaction of Na with O_3 in the nightglow process. Were there no ozone at all, we would see an intensity of around 5 R. With low level ozone, the intensity rises to about 25 R, indicating that the ozone reaction is at least a factor of four more important in producing the nightglow than is the three-body sequence. Increase of the ozone by a factor of ten increases the nightglow by about a factor of five. The increase is not linear because the process results in an overall decrease of free Na. Also, increase in ozone increases the non-radiative release of NaO through reaction 4. However, there is still a very strong correlation of the nightglow intensity with ozone density. In the next section, we will examine experimental evidence that might support this correlation.

5.0 SEASONAL VARIATIONS

Several extensive studies have been carried out on the variations of the sodium nightglow at various locations. One of the most comprehensive was carried out by *Fukuyama* [1977]. Among his results, was the demonstration of a strong latitude dependence of the seasonal variations in nightglow. At mid-latitudes in the northern hemisphere, where we will concentrate our own examination, he found a maximum monthly average of about 250 R in November to December and a minimum in mid-summer of about 50 R. Fukuyama's work is concerned mainly with Fourier analysis of the data and, as such, does not show the fine structure of the variations well.

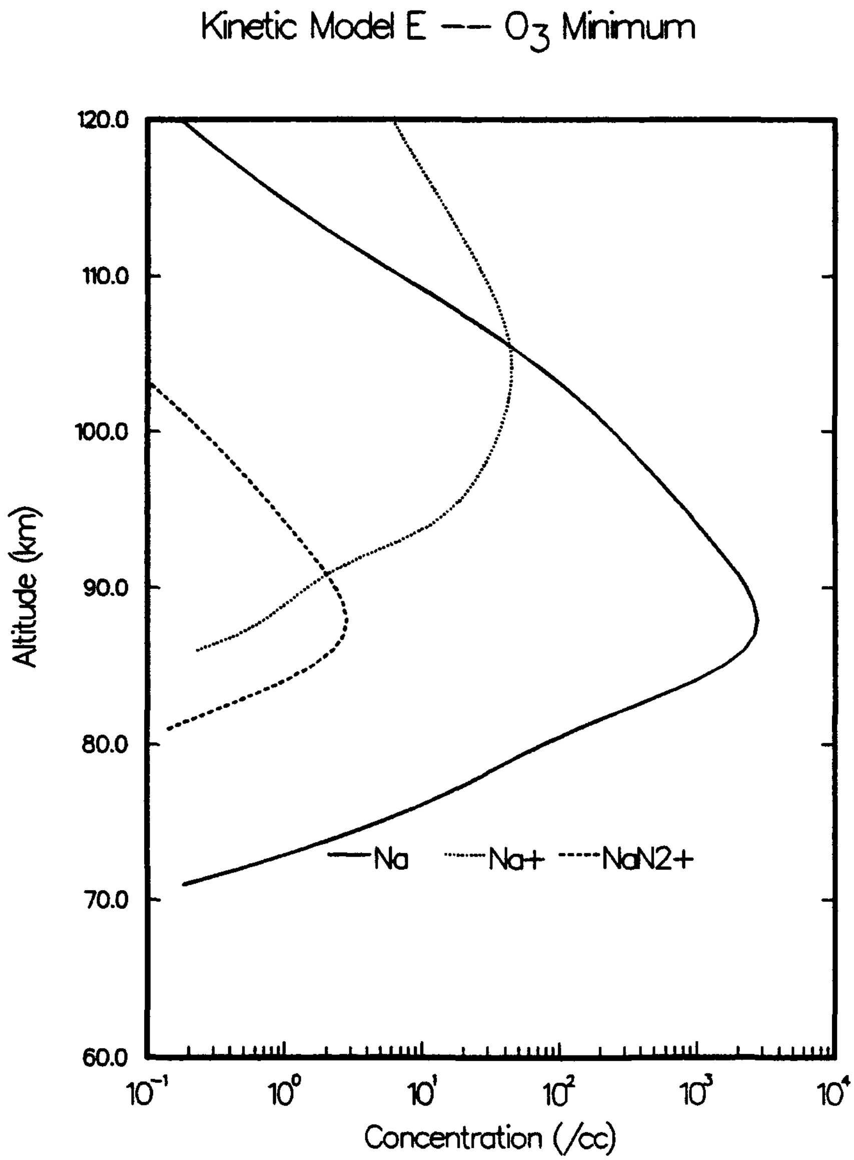

Figure 27. **The concentation of atomic sodium and sodium ions resulting from the solution of Kinetic Model E.**

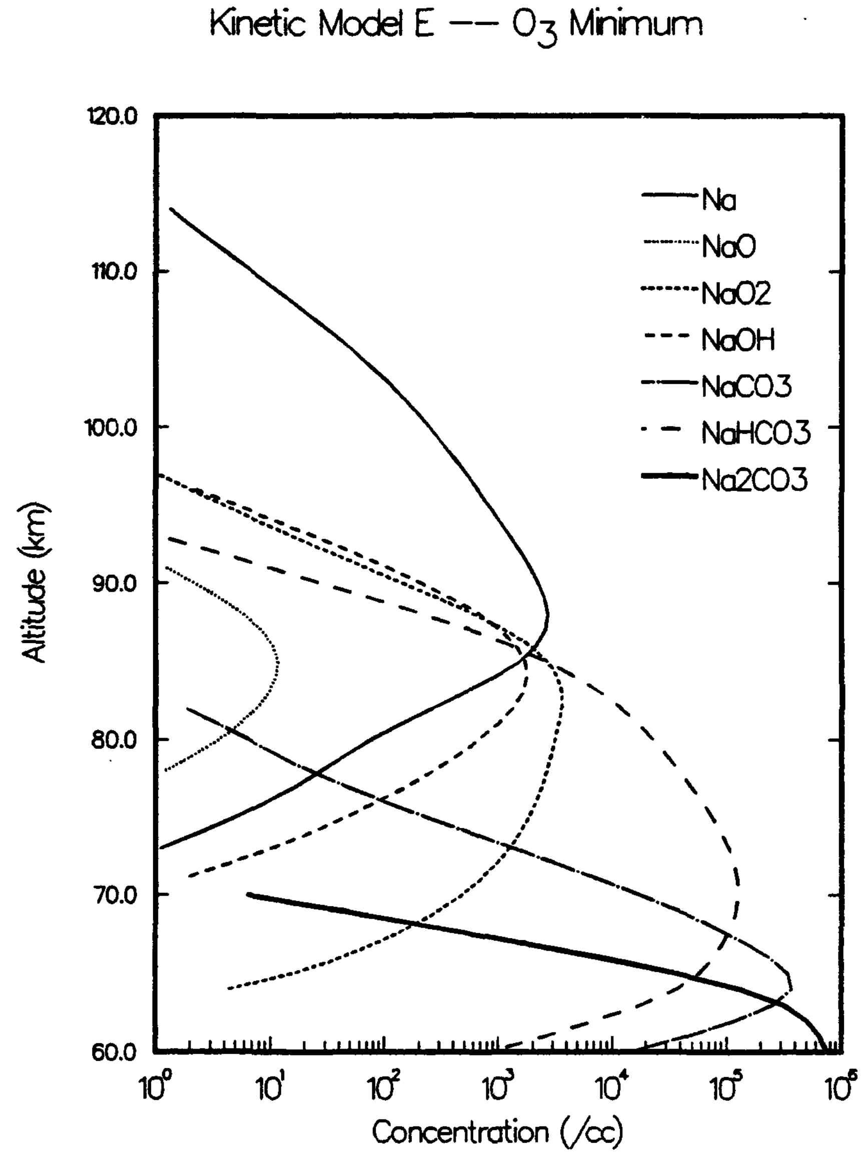

Figure 28. **The concentration of sodium neutral compounds resulting from the solution of Kinetic Model E.**

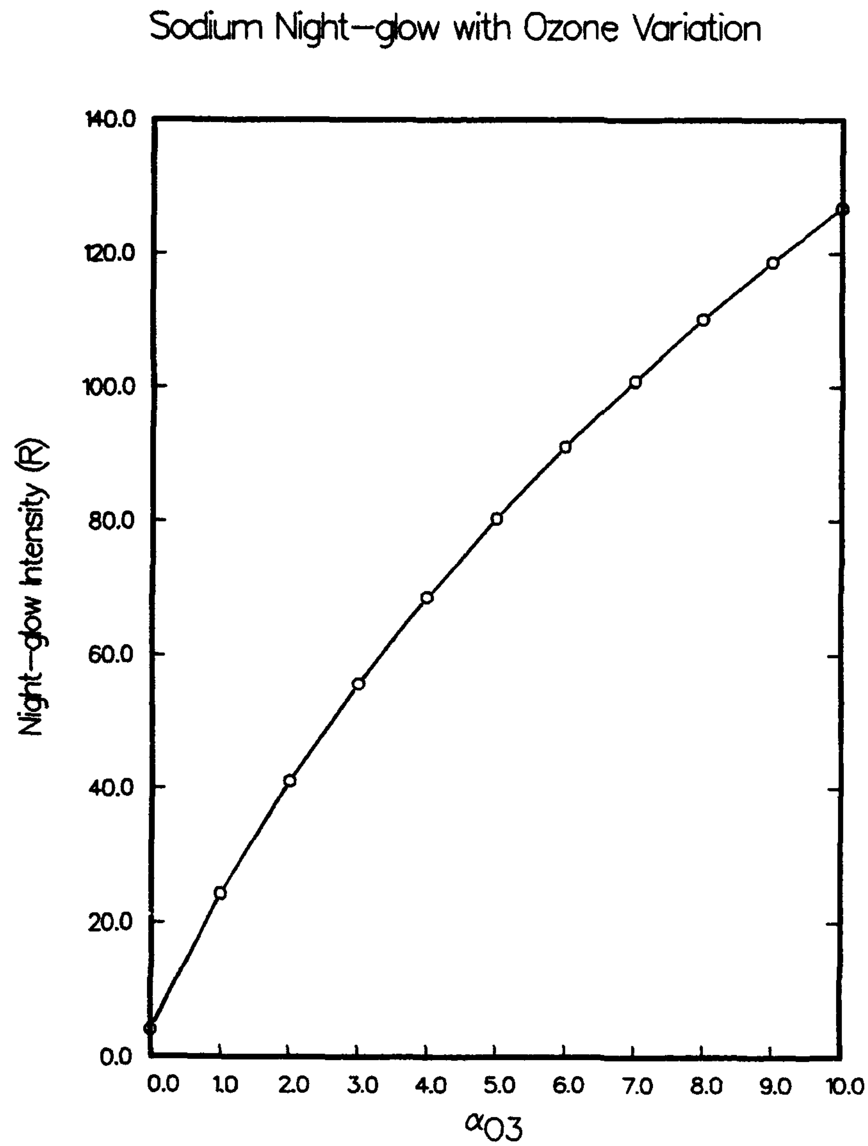

Figure 29. The variation in sodium nightglow with ozone concentration.

Table 9. Kinetic Model E

#	Reaction	Rate
1	$Na + O_3 \rightarrow NaO + O_2$	7.0(-10)
2	$NaO + O \rightarrow Na + O_2$	1.0(-10)
3	$NaO + O_3 \rightarrow NaO_2 + O_2$	2.0(-10)
4	$NaO + O_3 \rightarrow Na + 2O_2$	2.0(-11)
5	$NaO + H_2O \rightarrow NaOH + OH$	2.0(-10)
6	$NaO + O_2 + N_2 \rightarrow NaO_3 + N_2$	5.3(-30)
7	$NaO + CO_2 + N_2 \rightarrow NaCO_3 + N_2$	1.3(-27)
8	$Na + O_2 + N_2 \rightarrow NaO_2 + N_2$	2.0(-30)
9	$NaO_2 + O \rightarrow NaO + O_2$	1.0(-13)
10	$NaO_2 + H \rightarrow NaOH + O$	1.9(-14)
11	$NaOH + H \rightarrow Na + H_2O$	1.0(-11)
12	$NaOH + CO_2 + N_2 \rightarrow NaHCO_3$	1.9(-28)
13	$NaO_2 + OH \rightarrow NaOH + O_2$	1.0(-10)
14	$NaO_3 + O \rightarrow Na + 2O_2$	2.0(-14)
15	$NaO_3 + O \rightarrow NaO_2 + O_2$	2.0(-14)
16	$NaCO_3 + O \rightarrow NaO_2 + CO_2$	1.0(-11)
17	$NaCO_3 + H + N_2 \rightarrow NaHCO_3 + N_2$	1.0(-28)
18	$NaHCO_3 + H \rightarrow Na + H_2CO_3$	1.0(-11)
19	$NaO_2 + CO_2 + N_2 \rightarrow NaCO_3 + O + N_2$	1.0(-30)
20	$NaCO_3 + Na + N_2 \rightarrow Na_2CO_3 + N_2$	1.0(-28)
21	$Na_2CO_3 + O \rightarrow NaCO_3 + NaO$	1.0(-16)
22	$Na + O_2^+ \rightarrow Na^+ + O_2$	1.4(-9)
23	$Na + NO^+ \rightarrow Na^+ + NO$	1.0(-9)
24	$Na^+ + N_2 + N_2 \rightarrow NaN_2^+ + N_2$	2.5(-31)
25	$NaN_2^{\cdot} + e^- \rightarrow Na + N_2$	1.0(-6)

To take a closer look at the variations, we searched for data from original sources. Unfortunately, the bulk of the nightglow data was recorded two or three decades ago and much of it has been lost due to storage problems. However, we were able to locate about two years worth of data from a few stations in the early publications of World Data Center A in Boulder. These proved to be adequate for our purposes.

Figure 30 shows the combined data from 1964 and 1965, taken at Haute Province, France. Combining data is useful because there are often large gaps caused, presumably, because of cloudy conditions at the observation site. The year-to-year variations are actually quite consistent at the same station. We have also examined data from Kitt Peak, Arizona, and find that the qualitative agreement is very good, although latitude differences tend to reduce the intensity of the variations in the Kitt Peak data from those at the 45° north latitude of Haute Province.

The data show two striking features when processed with 31-day running averages. First, there are two strong peaks, one in late March to early April, and another in early November. These peaks are very similar from year to year and from station to station. We believe that these peaks, instead of being caused by variations in the ozone, are the results of increased meteoric activity. We do not have substantiating evidence for this belief at this point. However, we note that the generally accepted source for the grains that contribute most to the sodium in Earth's atmosphere is the release of dust from the evaporation of the ice in short period comets. According to *Encrenaz, et al.* [1989], Earth passes through the Lyrids meteor swarm from comet Thatcher on 10-20 April, and the Orinids from Halley, the Draconids from Giacobini-Zinner, and the Andromedids from Biela all in the mid-October to mid-November time span. It is of interest that passage through the Perseids swarm from comet Swift-Tuttle is not evident in Figure 30. However, comet Swift-Tuttle has a relatively long period of 125 years, and also a perihelion somewhat larger than 1 A.U. [*Hughes*, 1978]. This may mean that only the larger, and hence brighter particles reach Earth to give rise to the Perseids. We saw in Figure 5 that the bulk of the deposition comes from particles with mass of 1(-6) grams. Further, the ratio of solar radiation pressure to gravitational attraction goes as the reciprocal of the particle radius, so that smaller particles may be blown away, while heavier ones fall to the sun to be intercepted by Earth. We will leave off this speculation at this point, concluding only that the two peaks seem a fascinating subject for further study from the astronomical viewpoint.

More toward our purposes here, we note in Figure 30 that there is a strong sinusoidal variation in the nightglow, neglecting the two prominent peaks. The summer months exhibit a clear decrease in intensity to about the 20 R level while, in winter, the intensity averages about 140 R. This, we believe, is due to changes in the ozone density in the lower thermosphere. In order to investigate this possibility, we explored the seasonal variation in ozone. We began with examining the variation in total ozone. Figure 31 shows this variation as measured at a station near Haute Province at 43° north. This data has been averaged to form monthly averages over several years. As can be seen, there is a strong maximum in March and a minimum in August. This does not agree especially well with the nightglow trend evident in Figure 30. There are

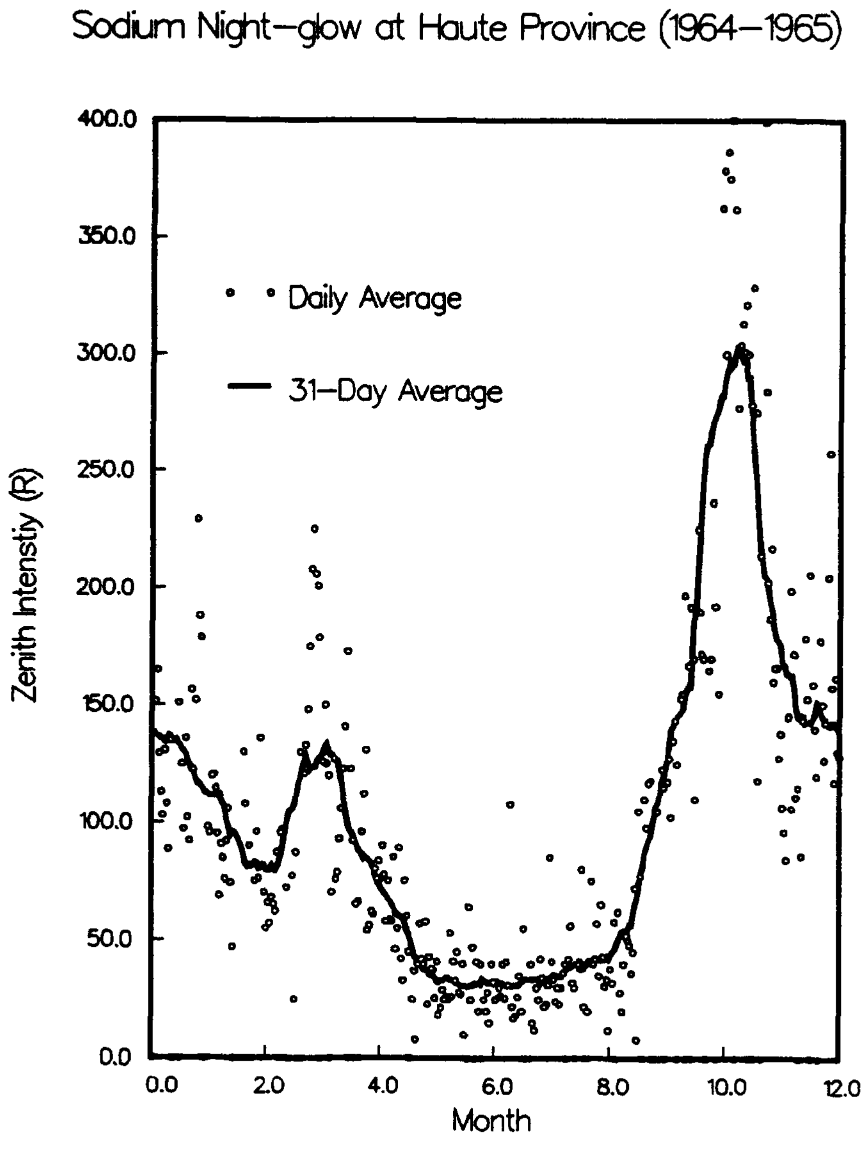

Figure 30. The seasonal variation in sodium nightglow measured at Haute Province, France, for 1964 and 1965.

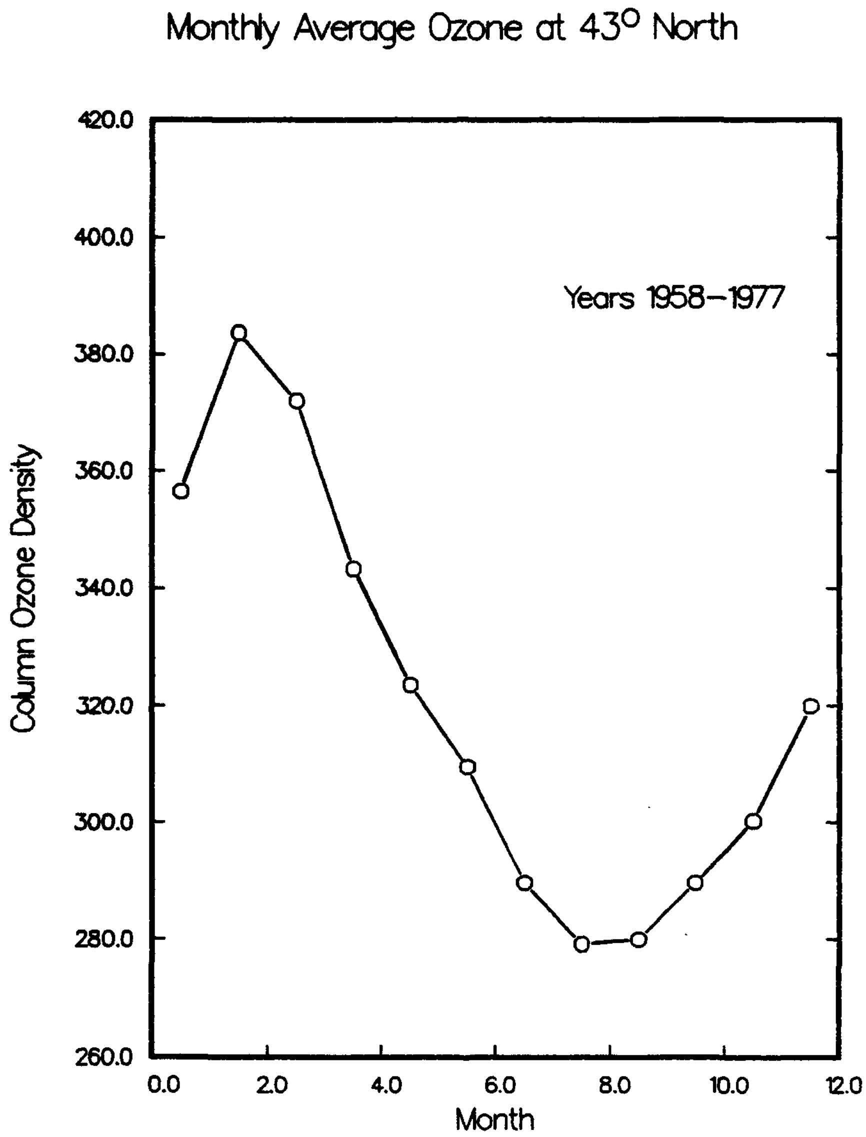

Figure 31. Seasonal Variation in monthly average column (total) ozone density measured at 43° N.

some good reasons for this. First, total ozone column density is measured in the daytime and extrapolated to local noon. The primary sink for ozone in the mesosphere and thermosphere in the daytime is photo-dissociation via the reaction

$$O_3 + h\nu \rightarrow O_2 + O(^1D) ,$$

while at night, the reaction with atomic hydrogen

$$O_3 + H \rightarrow OH + O_2$$

dominates completely. In the mesosphere and lower thermosphere, the night-time increase in ozone is something like a factor of 10, so that day measurements do not necessarily represent well the night situation where, necessarily, sodium night-glow measurements are made. The second reason why we might not expect good correlation of night-glow with total ozone is simply the fact that the total ozone is concentrated at lower altitudes. The bulk of the ozone column is in the stratosphere and, therefore, the amount at 90 km contributes negligibly to the total column density.

To substantiate the lack of correlation of total ozone with ozone at higher altitudes, we cite the work of *McPeters* [1980] who deduced the ozone concentration at 1 mbar pressure (about 65 km) from Nimbus 4 backscattered ultraviolet data. He found a winter peak of about 8 μg/g and a summer minimum of about 4 μg/g 50°N, a winter increase of a factor of two. This is almost exactly the opposite of the behavior of total ozone, which is a maximum in spring and a minimum in fall.

In fact, the current understanding of ozone density above 80 km appears at present to be sketchy and sometimes contradictory. The situation is complicated by the existence of a secondary maximum in O_3 at the mesopause, which seems to be quite variable with season, and even from day to day. There is also a general consensus [*see e.g. Allen, et al.*, 1984], that current models do not adequately predict the ozone density above 80 km altitude. Perhaps the most comprehensive results to date come from the analysis of 10 years of aircraft $O_2(^1\Delta)$ emissions in twilight, reported by *Noxon* [1981]. This author summarizes his results as follows:

> "Between 50 and 70 km there appears to be little variation ($< \pm 25\%$) whereas the abundance between 80 and 90 km exhibits a large seasonal change north of 30°N and much less at lower latitude. At mid and high latitude the column abundance above ~ 80 km changes from $< 1 \times 10^{14}$ cm^{-2} in summer to about 3×10^{14} cm^{-2} in winter."

Noxon made his conclusions by considering two models, a "low ozone" model which fit the decay in O_2 emissions (presumed to result from photolysis of O_3) as a function of zenith angle well in mid-summer, and a "high ozone" model which fit well in mid-winter. The author presents two curves, which we have modeled and which are shown in Figure 32. We have used these two curves to model the seasonal variation as follows.

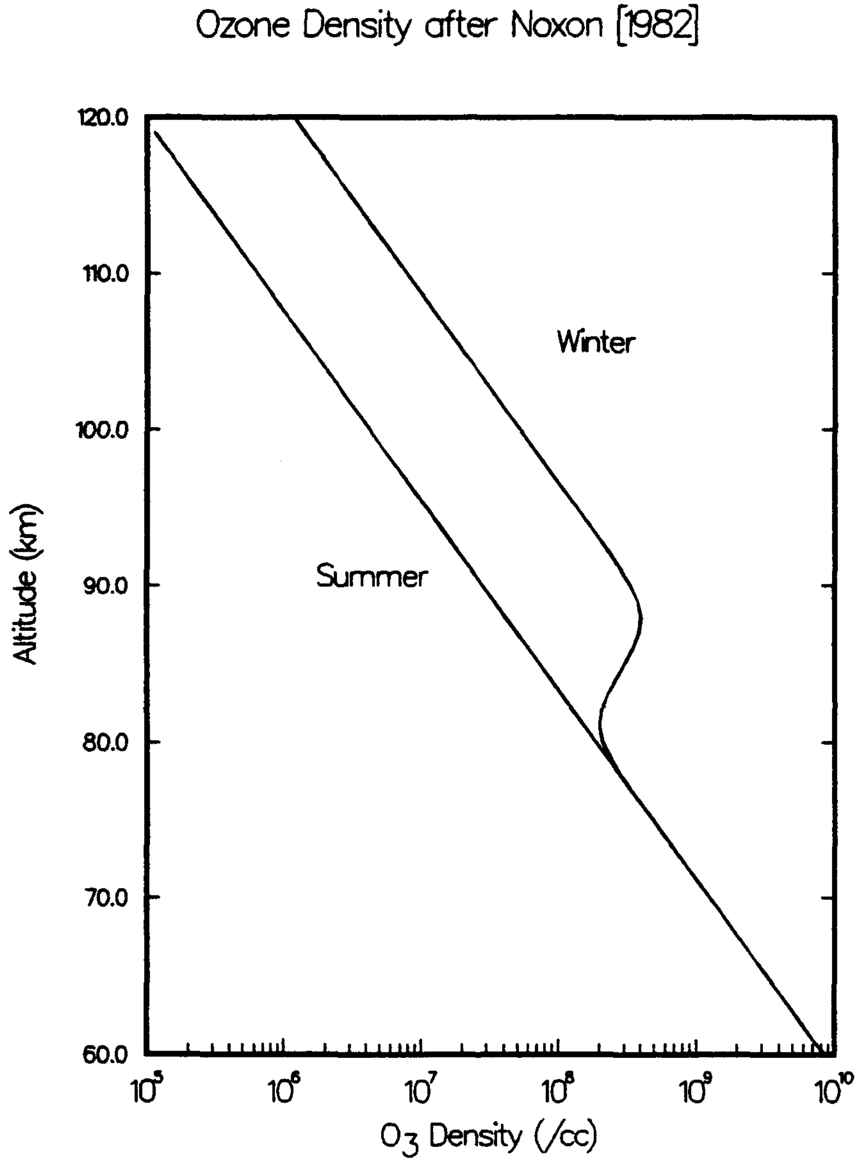

Figure 32. Minimum and maximum values of ozone density in the mesosphere and lower troposphere, modeled after the results of *Noxon* [1982].

$$n(O_3) = n_{summer}\sin^2\frac{2\pi m}{12} + n_{winter}\cos^2\frac{2\pi m}{12} \tag{18}$$

where m is the month. This model, when used to replace the O_3 density in Model E, gives rise to the nightglow variation shown in Figure 33. The variation is in remarkably good agreement with the variation in nightglow at Haute Province, shown in Figure 30, save again for the two peaks we believe to be due to meteor showers. The winter maximum is about 130 R, compared to perhaps 140 R in the Haute Province data, and the summer minimum is around 30 R in the model, compared to around 40 R in the data.

In Figure 34, we show the emission profile as a function of season, and Figure 35 shows the variation in the sodium layer caused by the variation in O_3. We see that the model predicts a slight lowering of the layer in the summer with a concurrent increase in sodium density. The increase is actually quite slight, amounting to about 20% in terms of column density. Megie and Blamount report that the sodium layer at Haute Province is actually quite constant, except for a rather sharp increase in late November. This increase would not seem to correlate with our model results, however, it could be due to the increase in meteoric activity since it does appear to correlate with the second anomalous peak in the nightglow data. The observed increase in free Na is more than a factor of 10, which is far too much to be explained by changes in the $[O_3]$.

There are at least two variables which we have omitted in this examination. One of these is temperature. The variation in temperature will affect the rates of all kinetic reactions and will also influence the thermal diffusion term in the diffusion equation. We do not rule out the possible influence of temperature effects, however, we believe from simple calculations that they would be of secondary importance. Finally, the nightglow and the sodium density are both strongly influenced by the atomic oxygen concentration. This is simply a result of the fact that the reaction between Na and O_3 is the rate limiting step in the Chapman process. The atomic hydrogen density is also of potential importance in replenishing free sodium. Unfortunately, neither of these is a particularly well known quantity. We believe that in view of the uncertainty in the rate coefficients used, the assumption of no seasonal variation in the atomic atmospheric species is reasonable. Also, the COSPAR International Reference Atmosphere of 1986, reports no seasonal variation of atomic oxygen at 90 km.

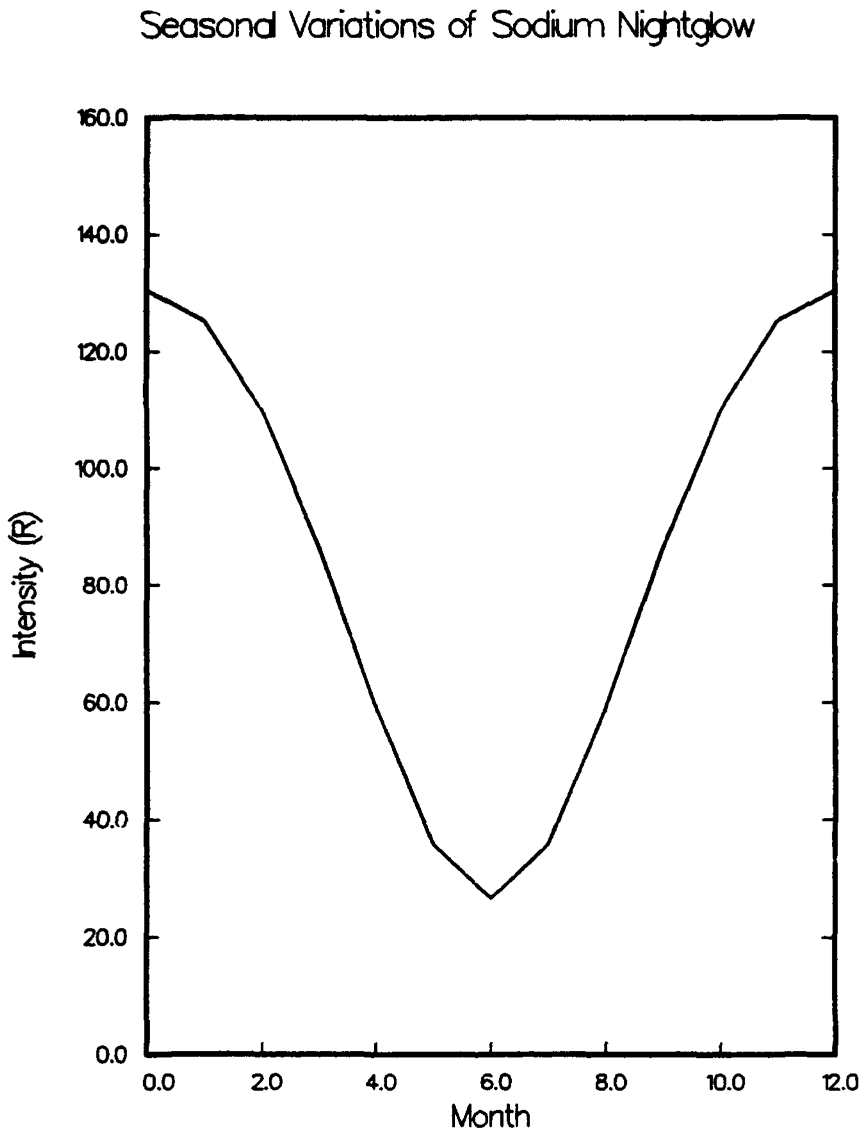

Figure 33. The seasonal variation in sodium nightglow calculated with Kinetic Model E and the variable ozone profiles in Figure 32.

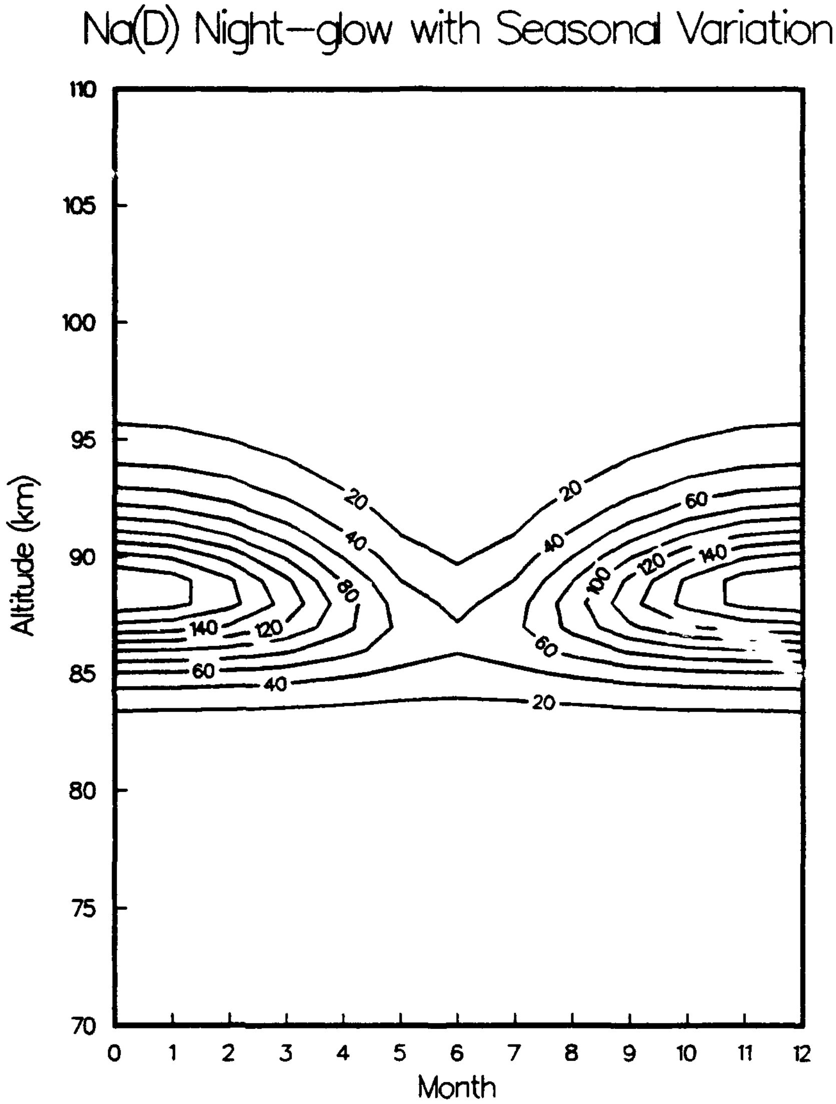

Figure 34. **The seasonal variation in the sodium nightglow layer (in photons/cm^3-s) using the modeled O_3 profiles.**

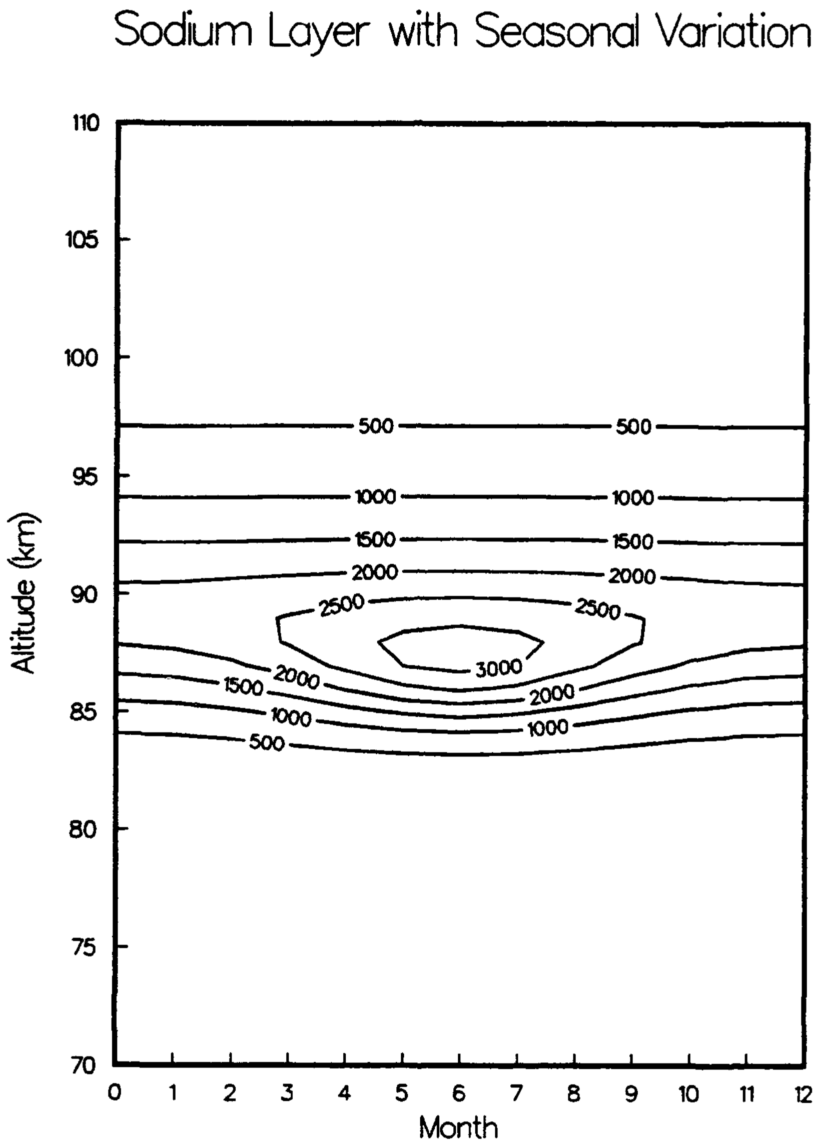

Figure 35. The seasonal variation in free sodium using the modeled O_3 profiles.

6.0 SUMMARY

We have developed a comprehensive model of atmospheric sodium deposition, beginning only with assumptions of the total mass deposition rate. The model yields a sodium layer that is in good agreement with experimental results. We have used the model to predict sodium nightglow intensity and have succeeded in duplicating the measured seasonal variation in that intensity by varying the lower tropospheric ozone in accordance with experimentally determined ozone minima and maxima. The results agree quite well with the measured nightglow at the 45°N station we examined.

The model itself is pleasing in that it is based to a large extent on first principles, beginning from an assumed and relatively well known mass input rate of cosmic dust to Earth's atmosphere. This model is equally valid for any other metallic species that arises from meteoric particle ablation and is valid without modification at any altitude. We intend to use the basic model to study the deposition of other metals and especially of ions at higher altitudes. As is generally the case, the introduction of a comprehensive kinetic scheme has required some assumptions about various rate constants. However, in this present model, we have obtained a scheme which is not strongly dependent on any of the precise rates for the "closure" reactions, the rates for which are not well known. The basic results of this model would remain the same with variation of rate constants within reasonable bounds.

Finally, the good correlation of modeled sodium nightglow with experimental results strongly supports the conclusion that lower thermospheric ozone abundance is the driving force in the seasonal variation in sodium nightglow. This result is important in that this region of the atmosphere is not well understood generally, and current models do not adequately predict the chemistry there. We believe that models such as this one, which attempt to identify causative agents for well known behavior, can contribute to a comprehensive understanding of the region.

REFERENCES

Allen, M, J.I. Lunine and Y.L. Yung, "The verticle distribution of ozone in the mesosphere and lower thermosphere", *J. Geophys. Res.*, **89**, 4841 (1984).

Banks, P.M., and G. Kockarts, "Aeronomy", Academic Press, Inc., New York (1973).

Bates, D.R., and P.C. Ojha, "Excitation of the Na D-doublet of the nightglow", *Nature*, **286**, 790 (1980).

Chapman, S., "Notes on atmospheric ozone", *Astrophys. J.*, **90**, 309 (1939).

Encrenaz, T., J.-P. Bibring and M. Blanc, "The Solar System", Springer-Verlag, Berlin, 1989.

Fukukama, K, "Airglow variations and dynamics in the lower thermosphere and upper mesosphere-II. Seasonal and long-term variations", *J. Atmosphere. Terr. Phys.*, **39**, 1 (1977).

Hughes, D.W., "Cosmic Dust Influx to the Earth", *Space Research XV*, Akademie-Verlag, Berlin, 1975.

Hughes, D.W., "Cosmic Dust", J.C. McDonnel, ed., John Wiley and Sons, 1978.

Hughes, D.W., "The meteorite flux", *Space Science Reviews*, **61**, 275 (1992).

Hunten, D.M., R.P. Turco and O.B. Toon, "Smoke and dust particles of meteoric origin in the mesosphere and stratosphere", *J. Atmos. Sci.*, **37**, 1342 (1980).

Kelley, M.C., "The Earth's Ionosphere", International Geophysics Series, **43**, Academic Press, New York (1989).

Keneshea, T.J., S.P. Zimmerman and C.R. Philbrick, "A dynamic model of the mesosphere and lower thermosphere", *Planet. Space Sci.*, **27**, 385 (1979).

McPeters, R.D., "The behavior of ozone near the stratopause from two years of BUV observations", *J. Geophys. Res.*, **85c**, 4545 (1980).

Noxon, J.F., "Global study of O_2 airglow: day and twilight", *Planet. Space Sci.*, **30**, 545, 1982.

Plane, J.M.C., "The chemistry of meteoric metals in the Earth's upper atmosphere", *International Reviews in Physical Chemistry*, **10**, 55 (1991).

Sze, N.D., M.K.W.Ko, W. Swider and E. Murad, "Atmospheric sodium chemistry I, The altitude region 70-100 km", *Geophys. Res. Lett.*, **9**, 1187 (1982).

Swider, W., "Sodium Nightglow: Chemically Independent of Sodium Content", *J. Geophys. Res.*, **91**, 6742 (1986).

Thomas, L., M.C. Isherwood and M.R. Bowman, "A theoretical study of the height distribution of sodium in the mesosphere", *J. Atmosph. Terr. Phys.*, **45**, 587 (1983).

Tilger, C. and U. von Zahn, *J. Geophys. Res.*, **93**, 8439 (1988).

Thomas, R.J., "Total Mixing Ratios", *Planet. Space Sci*, **22**, 175 (1974).

APPENDIX. KINETIC MODEL SOLUTION METHOD

The problem of solving the steady state kinetic models rapidly becomes complicated with an increasing number of reactions and constituents. We have written a program called KINO which assists in this task. The routine takes as input a file describing the kinetic model. The file for the most complicated model used in this investigation, Model E, is shown below.

```
SODIUM MODEL E
01) Na + O3 = NaO + O2                          $   7.0E-10
02) NaO + O = Na + O2                           $   1.0E-10
03) NaO + O3 = NaO2 + O2                        $   2.0E-10
04) NaO + O3 = Na + O2 + O2                     $   2.0E-11
05) NaO + H2O = NaOH + OH                       $   2.0E-10
06) NaO + O2 + N2 = NaO3 + N2                   $   5.3E-30
07) NaO + CO2 + N2 = NaCO3 + N2                 $   1.3E-27
08) Na + O2 + N2 = NaO2 + N2                    $   2.0E-30
09) Na + O2+ = Na+ + O2                         $   1.4E-9
10) Na + NO+ = Na+ + NO                         $   1.0e-9
11) Na+ + N2 + N2 = NaN2+ + N2                  $   2.5e-31
12) NaN2+ + e- = Na + N2                        $   1.0e-6
13) NaO2 + O = NaO + O2                         $   1.0E-13
14) NaO2 + H = NaOH + O                         $   1.9E-14
15) NaOH + H = Na + H2O                         $   1.0e-11
16) NaOH + CO2 + N2 = NaHCO3 + N2               $   1.9E-28
17) NaO2 + OH = NaOH + O2                       $   1.0E-10
18) NaO3 + O = Na + O2 + O2                     $   2.0E-14
19) NaO3 + O = NaO2 + O2                        $   2.0E-14
20) NaCO3 + O = NaO2 + CO2                      $   1.0E-11
21) NaCO3 + H + N2 = NaHCO3 + N2                $   1.0E-28
22) NaHCO3 + H = Na + H2CO3                     $   1.0E-11
23) NaO2 + CO2 + N2 = NaCO3 + O + N2            $   1.0E-30
24) NaCO3 + Na + N2 = Na2CO3 + N2               $   1.0E-28
25) Na2CO3 + O = NaO + NaCO3                    $   1.0E-16
```

The input file contains a line consisting of the reactants and products, which are separated by an '=' sign. After these, a '$' sign indicates that the next value is the rate coefficient. The KINO program reads this file and tallies up all reactants and products along with the appropriate rate constant. The program is perhaps best described by showing its various output.

The first output is a list of all *different* species encountered in the input file. Along with this, is an indication of which reactions these species are involved in. The list below corresponds to the input file above. A second table (not shown in this output) keeps tracks of how many of each species are created and/or destroyed by each reaction.

Sp.	1	Na	1	0	0	0	0	0	0	1	1	1	0	0	0	0	0	0	0	0	0	0	0	0	0	1	0
Sp.	2	O3	1	0	1	1	0	0	0	0	0	0	0	0	0	0	0	0	0	0	0	0	0	0	0	0	0
Sp.	3	NaO	0	1	1	1	1	1	1	0	0	0	0	0	0	0	0	0	0	0	0	0	0	0	0	0	0
Sp.	4	O2	0	0	0	0	0	1	0	1	0	0	0	0	0	0	0	0	0	0	0	0	0	0	0	0	0
Sp.	5	O	0	1	0	0	0	0	0	0	0	0	0	0	1	0	0	0	0	1	1	1	0	0	0	0	1
Sp.	6	NaO2	0	0	0	0	0	0	0	0	0	0	0	0	1	1	0	0	1	0	0	0	0	0	1	0	0
Sp.	7	H2O	0	0	0	0	1	0	0	0	0	0	0	0	0	0	0	0	0	0	0	0	0	0	0	0	0
Sp.	8	NaOH	0	0	0	0	0	0	0	0	0	0	0	0	0	0	1	1	0	0	0	0	0	0	0	0	0
Sp.	9	OH	0	0	0	0	0	0	0	0	0	0	0	0	0	0	0	0	1	0	0	0	0	0	0	0	0
Sp.	10	N2	0	0	0	0	0	1	1	1	0	0	2	0	0	0	0	1	0	0	0	0	1	0	1	1	0
Sp.	11	NaO3	0	0	0	0	0	0	0	0	0	0	0	0	0	0	0	0	0	1	1	0	0	0	0	0	0
Sp.	12	CO2	0	0	0	0	0	0	1	0	0	0	0	0	0	0	0	1	0	0	0	0	0	0	1	0	0
Sp.	13	NaCO3	0	0	0	0	0	0	0	0	0	0	0	0	0	0	0	0	0	0	0	1	1	0	0	1	0
Sp.	14	O2+	0	0	0	0	0	0	0	0	1	0	0	0	0	0	0	0	0	0	0	0	0	0	0	0	0
Sp.	15	Na+	0	0	0	0	0	0	0	0	0	0	1	0	0	0	0	0	0	0	0	0	0	0	0	0	0
Sp.	16	NO+	0	0	0	0	0	0	0	0	0	1	0	0	0	0	0	0	0	0	0	0	0	0	0	0	0
Sp.	17	NO	0	0	0	0	0	0	0	0	0	0	0	0	0	0	0	0	0	0	0	0	0	0	0	0	0
Sp.	18	NaN2+	0	0	0	0	0	0	0	0	0	0	0	1	0	0	0	0	0	0	0	0	0	0	0	0	0
Sp.	19	e-	0	0	0	0	0	0	0	0	0	0	0	1	0	0	0	0	0	0	0	0	0	0	0	0	0
Sp.	20	H	0	0	0	0	0	0	0	0	0	0	0	0	0	1	1	0	0	0	0	0	1	1	0	0	0
Sp.	21	NaHCO3	0	0	0	0	0	0	0	0	0	0	0	0	0	0	0	0	0	0	0	0	0	1	0	0	0
Sp.	22	H2CO3	0	0	0	0	0	0	0	0	0	0	0	0	0	0	0	0	0	0	0	0	0	0	0	0	0
Sp.	23	Na2CO3	0	0	0	0	0	0	0	0	0	0	0	0	0	0	0	0	0	0	0	0	0	0	0	0	1

After presenting this table, the program can do a mass check and charge check to make sure there have been no typos in the input file. The results are given below. Charge is indicated in the file by a '+' or a '-' following the species in the input file.

FINISHED WITH INPUT
DO YOU WANT A CHARGE BALANCE CHECK?(1=YES)

CHECKING CHARGE BALANCE ...

SPECIES	***1***	***Na***	***CHARGE***	***0***
SPECIES	***2***	***03***	***CHARGE***	***0***
SPECIES	***3***	***NaO***	***CHARGE***	***0***
SPECIES	***4***	***02***	***CHARGE***	***0***
SPECIES	***5***	***O***	***CHARGE***	***0***
SPECIES	***6***	***Na02***	***CHARGE***	***0***
SPECIES	***7***	***H2O***	***CHARGE***	***0***
SPECIES	***8***	***NaOH***	***CHARGE***	***0***
SPECIES	***9***	***OH***	***CHARGE***	***0***
SPECIES	***10***	***N2***	***CHARGE***	***0***
SPECIES	***11***	***Na03***	***CHARGE***	***0***
SPECIES	***12***	***CO2***	***CHARGE***	***0***
SPECIES	***13***	***NaCO3***	***CHARGE***	***0***
SPECIES	***14***	***02+***	***CHARGE***	***1***
SPECIES	***15***	***Na+***	***CHARGE***	***1***
SPECIES	***16***	***NO+***	***CHARGE***	***1***
SPECIES	***17***	***NO***	***CHARGE***	***0***
SPECIES	***18***	***NaN2+***	***CHARGE***	***1***
SPECIES	***19***	***e-***	***CHARGE***	***-1***
SPECIES	***20***	***H***	***CHARGE***	***0***
SPECIES	***21***	***NaHCO3***	***CHARGE***	***0***

```
SPECIES  22   H2CO3        CHARGE  0
SPECIES  23   Na2CO3       CHARGE  0
RXN.  1 Na + O3 = NaO + O2                      CHARGE  0
RXN.  2 NaO + O = Na + O2                       CHARGE  0
RXN.  3 NaO + O3 = NaO2 + O2                    CHARGE  0
RXN.  4 NaO + O3 = Na + O2 + O2                 CHARGE  0
RXN.  5 NaO + H2O = NaOH + OH                   CHARGE  0
RXN.  6 NaO + O2 + N2 = NaO3 + N2               CHARGE  0
RXN.  7 NaO + CO2 + N2 = NaCO3 + N2             CHARGE  0
RXN.  8 Na + O2 + N2 = NaO2 + N2                CHARGE  0
RXN.  9 Na + O2+ = Na+ + O2                     CHARGE  0
RXN. 10 Na + NO+ = Na+ + NO                     CHARGE  0
RXN. 11 Na+ + N2 + N2 = NaN2+ + N2              CHARGE  0
RXN. 12 NaN2+ + e- = Na + N2                    CHARGE  0
RXN. 13 NaO2 + O = NaO + O2                     CHARGE  0
RXN. 14 NaO2 + H = NaOH + O                     CHARGE  0
RXN. 15 NaOH + H = Na + H2O                     CHARGE  0
RXN. 16 NaOH + CO2 + N2 = NaHCO3 + N2           CHARGE  0
RXN. 17 NaO2 + OH = NaOH + O2                   CHARGE  0
RXN. 18 NaO3 + O = Na + O2 + O2                 CHARGE  0
RXN. 19 NaO3 + O = NaO2 + O2                    CHARGE  0
RXN. 20 NaCO3 + O = NaO2 + CO2                  CHARGE  0
RXN. 21 NaCO3 + H + N2 = NaHCO3 + N2            CHARGE  0
RXN. 22 NaHCO3 + H = Na + H2CO3                 CHARGE  0
RXN. 23 NaO2 + CO2 + N2 = NaCO3 + O + N2        CHARGE  0
RXN. 24 NaCO3 + Na + N2 = Na2CO3 + N2           CHARGE  0
RXN. 25 Na2CO3 + O = NaO + NaCO3                CHARGE  0

DO YOU WANT A MASS BALANCE CHECK?(1=YES)

Sp.  1  Na        Mass  22
Sp.  2  O3        Mass  48
Sp.  3  NaO       Mass  38
Sp.  4  O2        Mass  32
Sp.  5  O         Mass  16
Sp.  6  NaO2      Mass  54
Sp.  7  H2O       Mass  18
Sp.  8  NaOH      Mass  39
Sp.  9  OH        Mass  17
Sp. 10  N2        Mass  28
Sp. 11  NaO3      Mass  70
Sp. 12  CO2       Mass  44
Sp. 13  NaCO3     Mass  82
Sp. 14  O2+       Mass  32
```

Sp. 15	*Na+*	*Mass*	*22*
Sp. 16	*NO+*	*Mass*	*30*
Sp. 17	*NO*	*Mass*	*30*
Sp. 18	*NaN2+*	*Mass*	*50*
Sp. 19	*e-*	*Mass*	*0*
Sp. 20	*H*	*Mass*	*1*
Sp. 21	*NaHCO3*	*Mass*	*83*
Sp. 22	*H2CO3*	*Mass*	*62*
Sp. 23	*Na2CO3*	*Mass*	*104*

RXN. 1	*Na + O3 = NaO + O2*	*MASS*	*0*
RXN. 2	*NaO + O = Na + O2*	*MASS*	*0*
RXN. 3	*NaO + O3 = NaO2 + O2*	*MASS*	*0*
RXN. 4	*NaO + O3 = Na + O2 + O2*	*MASS*	*0*
RXN. 5	*NaO + H2O = NaOH + OH*	*MASS*	*0*
RXN. 6	*NaO + O2 + N2 = NaO3 + N2*	*MASS*	*0*
RXN. 7	*NaO + CO2 + N2 = NaCO3 + N2*	*MASS*	*0*
RXN. 8	*Na + O2 + N2 = NaO2 + N2*	*MASS*	*0*
RXN. 9	*Na + O2+ = Na+ + O2*	*MASS*	*0*
RXN. 10	*Na + NO+ = Na+ + NO*	*MASS*	*0*
RXN. 11	*Na+ + N2 + N2 = NaN2+ + N2*	*MASS*	*0*
RXN. 12	*NaN2+ + e- = Na + N2*	*MASS*	*0*
RXN. 13	*NaO2 + O = NaO + O2*	*MASS*	*0*
RXN. 14	*NaO2 + H = NaOH + O*	*MASS*	*0*
RXN. 15	*NaOH + H = Na + H2O*	*MASS*	*0*
RXN. 16	*NaOH + CO2 + N2 = NaHCO3 + N2*	*MASS*	*0*
RXN. 17	*NaO2 + OH = NaOH + O2*	*MASS*	*0*
RXN. 18	*NaO3 + O = Na + O2 + O2*	*MASS*	*0*
RXN. 19	*NaO3 + O = NaO2 + O2*	*MASS*	*0*
RXN. 20	*NaCO3 + O = NaO2 + CO2*	*MASS*	*0*
RXN. 21	*NaCO3 + H + N2 = NaHCO3 + N2*	*MASS*	*0*
RXN. 22	*NaHCO3 + H = Na + H2CO3*	*MASS*	*0*
RXN. 23	*NaO2 + CO2 + N2 = NaCO3 + O + N2*	*MASS*	*0*
RXN. 24	*NaCO3 + Na + N2 = Na2CO3 + N2*	*MASS*	*0*
RXN. 25	*Na2CO3 + O = NaO + NaCO3*	*MASS*	*0*

The mass is determined by adding up all species in each reaction, and a zero total mass for each reaction indicates a valid reaction, as does a zero total charge. After this output, the routine can write either a time-dependent subroutine using Runge-Kutta or a steady state routine. For the steady state routine, a matrix is generated. To understand the matrix concept, consider the following simple reaction scheme.

$$Na + O_3 \rightarrow NaO + O2$$
$$NaO + O \rightarrow Na + O2$$

In this simple scheme, there are two NaX species, Na and NaO. The steady state equations can thus be written

$$\frac{d[Na]}{dt} = 0 = -k_1[Na][O_3] + k_2[NaO][O]$$

$$\frac{d[NaO]}{dt} = 0 = k_1[Na][O_3] - k_2[NaO][O]$$

Although this case is trivial to solve, we see that the problem can be written in the form of linear system in which the elements of an array a_{ii} are the sums of all reaction rates that remove the component i from the system, and the a_{ij} are the sums of all those that change component j into component i. We can also see that the system is overdetermined, since we can multiply all the components by a scaler and still have a solution.

$$\begin{bmatrix} a_{11} & a_{12} & a_{13} \\ a_{21} & a_{22} & a_{23} \\ a_{31} & a_{32} & a_{33} \end{bmatrix} \begin{bmatrix} n_1 \\ n_2 \\ n_3 \end{bmatrix} = [0]$$

The equation above represents a three-component steady state matrix. To solve the problem, we take the value of one of the components, n_1, to be unity. Then, we solve the n-1 linear equation to find the components n_2, n_3,....n_n. Finally, knowing the total of all components, we can normalize the solution. The KINO program writes a subroutine which fills up a matrix, such as the one above. A sample subroutine corresponding to Model E is given below. In that routine, the species that must be specified externally, *i.e.* the constant components of the atmosphere in this case, are listed and must be supplied to the routine through common statements. The KINO program asks the user for a string, in this case 'Na', by which it may differentiate constant constituents from variable constituents.

```
      SUBROUTINE FILLMAT(AMAT)
C
      IMPLICIT REAL*8 (A-H,O-Z)
C
      DIMENSION AMAT(10,10)
C
```

```
C  THE FOLLOWING ARE VARIABLES IN THE PROBLEM
C
C     1   2 Na
C     2   3 NaO
C     3   4 NaO2
C     4   5 NaOH
C     5   6 NaO3
C     6   7 NaCO3
C     7   8 Nap
C     8   9 NaN2p
C     9  10 NaHCO3
C    10  11 Na2CO3
C
C THE FOLLOWING DENSITIES MUST BE SUPPLIED
C
C  O3
C  O2
C  O
C  H2O
C  OH
C  N2
C  CO2
C  O2p
C  NOp
C  em
C  H
C
C THE FOLLOWING REACTIONS ARE INCLUDED
C
C  1. Na + O3 = NaO + O2
C  2. NaO + O = Na + O2
C  3. NaO + O3 = NaO2 + O2
C  4. NaO + O3 = Na + O2 + O2
C  5. NaO + H2O = NaOH + OH
C  6. NaO + O2 + N2 = NaO3 + N2
C  7. NaO + CO2 + N2 = NaCO3 + N2
C  8. Na + O2 + N2 = NaO2 + N2
C  9. Na + O2+ = Na+ + O2
C 10. Na + NO+ = Na+ + NO
C 11. Na+ + N2 + N2 = NaN2+ + N2
C 12. NaN2+ + e- = Na + N2
C 13. NaO2 + O = NaO + O2
C 14. NaO2 + H = NaOH + O
C 15. NaOH + H = Na + H2O
```

```
C  16.  NaOH + CO2 + N2 = NaHCO3 + N2
C  17.  NaO2 + OH = NaOH + O2
C  18.  NaO3 + O = Na + O2 + O2
C  19.  NaO3 + O = NaO2 + O2
C  20.  NaCO3 + O = NaO2 + CO2
C  21.  NaCO3 + H + N2 = NaHCO3 + N2
C  22.  NaHCO3 + H = Na + H2CO3
C  23.  NaO2 + CO2 + N2 = NaCO3 + O + N2
C  24.  NaCO3 + Na + N2 = Na2CO3 + N2
C  25.  Na2CO3 + O = NaO + NaCO3
C
      REAL*8 O3
      REAL*8 O2
      REAL*8 O
      REAL*8 H2O
      REAL*8 OH
      REAL*8 N2
      REAL*8 CO2
      REAL*8 O2p
      REAL*8 NOp
      REAL*8 em
      REAL*8 H
C
      O3=DO3
      O2=DO2
      O=DO
      H2O=DH2O
      OH=DOH
      N2=DN2
      CO2=DCO2
      O2p=DO2p
      NOp=DNOp
      em=Dem
      H=DH
C
      R01=  7.0000E-10
      R02=  1.0000E-10
      R03=  2.0000E-10
      R04=  2.0000E-11
      R05=  2.0000E-10
      R06=  5.3000E-30
      R07=  1.3000E-27
      R08=  2.0000E-30
      R09=  1.4000E-09
```

```
      R10=  1.0000E-09
      R11=  2.5000E-31
      R12=  1.0000E-06
      R13=  1.0000E-13
      R14=  1.9000E-14
      R15=  1.0000E-11
      R16=  1.9000E-28
      R17=  1.0000E-10
      R18=  2.0000E-14
      R19=  2.0000E-14
      R20=  1.0000E-11
      R21=  1.0000E-28
      R22=  1.0000E-11
      R23=  1.0000E-30
      R24=  1.0000E-28
      R25=  1.0000E-16
C
      AMAT(01,01)=-R01*O3-R08*O2*N2-R09*O2p-R10*NOp-R24*N2
      AMAT(01,02)=+R02*O+R04*O3
      AMAT(01,03)=0.0
      AMAT(01,04)=+R15*H
      AMAT(01,05)=+R18*O
      AMAT(01,06)=0.0
      AMAT(01,07)=0.0
      AMAT(01,08)=+R12*em
      AMAT(01,09)=+R22*H
      AMAT(01,10)=0.0
      AMAT(02,01)=+R01*O3
      AMAT(02,02)=-R02*O-R03*O3-R04*O3-R05*H2O-R06*O2*N2-R07*N2*CO2
      AMAT(02,03)=+R13*O
      AMAT(02,04)=0.0
      AMAT(02,05)=0.0
      AMAT(02,06)=0.0
      AMAT(02,07)=0.0
      AMAT(02,08)=0.0
      AMAT(02,09)=0.0
      AMAT(02,10)=+R25*O
      AMAT(03,01)=+R08*O2*N2
      AMAT(03,02)=+R03*O3
      AMAT(03,03)=-R13*O-R14*H-R17*OH-R23*N2*CO2
      AMAT(03,04)=0.0
      AMAT(03,05)=+R19*O
      AMAT(03,06)=+R20*O
      AMAT(03,07)=0.0
```

```
AMAT(03,08)=0.0
AMAT(03,09)=0.0
AMAT(03,10)=0.0
AMAT(04,01)=0.0
AMAT(04,02)= +R05*H2O
AMAT(04,03)= +R14*H+R17*OH
AMAT(04,04)=-R15*H-R16*N2*CO2
AMAT(04,05)=0.0
AMAT(04,06)=0.0
AMAT(04,07)=0.0
AMAT(04,08)=0.0
AMAT(04,09)=0.0
AMAT(04,10)=0.0
AMAT(05,01)=0.0
AMAT(05,02)= +R06*O2*N2
AMAT(05,03)=0.0
AMAT(05,04)=0.0
AMAT(05,05)=-R18*O-R19*O
AMAT(05,06)=0.0
AMAT(05,07)=0.0
AMAT(05,08)=0.0
AMAT(05,09)=0.0
AMAT(05,10)=0.0
AMAT(06,01)=0.0
AMAT(06,02)= +R07*N2*CO2
AMAT(06,03)= +R23*N2*CO2
AMAT(06,04)=0.0
AMAT(06,05)=0.0
AMAT(06,06)=-R20*O-R21*N2*H-R24*N2
AMAT(06,07)=0.0
AMAT(06,08)=0.0
AMAT(06,09)=0.0
AMAT(06,10)= +R25*O
AMAT(07,01)= +R09*O2p+R10*NOp
AMAT(07,02)=0.0
AMAT(07,03)=0.0
AMAT(07,04)=0.0
AMAT(07,05)=0.0
AMAT(07,06)=0.0
AMAT(07,07)=-R11*N2*N2
AMAT(07,08)=0.0
AMAT(07,09)=0.0
AMAT(07,10)=0.0
AMAT(08,01)=0.0
```

```
      AMAT(08,02)=0.0
      AMAT(08,03)=0.0
      AMAT(08,04)=0.0
      AMAT(08,05)=0.0
      AMAT(08,06)=0.0
      AMAT(08,07)= +R11*N2*N2
      AMAT(08,08)=-R12*em
      AMAT(08,09)=0.0
      AMAT(08,10)=0.0
      AMAT(09,01)=0.0
      AMAT(09,02)=0.0
      AMAT(09,03)=0.0
      AMAT(09,04)= +R16*N2*CO2
      AMAT(09,05)=0.0
      AMAT(09,06)= +R21*N2*H
      AMAT(09,07)=0.0
      AMAT(09,08)=0.0
      AMAT(09,09)=-R22*H
      AMAT(09,10)=0.0
      AMAT(10,01)= +R24*N2
      AMAT(10,02)=0.0
      AMAT(10,03)=0.0
      AMAT(10,04)=0.0
      AMAT(10,05)=0.0
      AMAT(10,06)= +R24*N2
      AMAT(10,07)=0.0
      AMAT(10,08)=0.0
      AMAT(10,09)=0.0
      AMAT(10,10)=-R25*O
C
      RETURN
      END
```